UCLouvain

École polytechnique de Louvain

Viscoelastic properties of polymer blends under elongation

Author : **Thomas Payon**
Supervisor : **Evelyne van Ruymbeke**
Readers : **Charles-André Fustin**, **Thomas Pardoen**, **Pascal Van Velthem**
Academic year 2023–2024
Master [120] in Chemical and Materials Engineering

Acknowledgements

I cannot begin this work without thanking the people who supported me during this final study project and whose help was invaluable.

First, I want to express my gratitude towards my supervisor, Professor Evelyne van Ruymbeke, for always being there to help me and for working hard to support me. Her advice and the time she spent with me were really important for making my work better.

I also want to thank Professors Charles-André Fustin, Thomas Pardoen, and Pascal Van Velthem for the time devoted to reading this work. I'm also grateful to Professor Pascal Van Velthem for helping me with the DSC analyses. His knowledge and help were really important.

I also want to thank Céline Hannecart, for helping me a lot when I was starting out with my experiments. Her help and advice were really important for getting and understanding the results.

I want to say a special thank you to Tiffanie, my partner, for always supporting me. Their encouragement for me made a big difference.

Finally, I want to thank all my colleagues in the lab for making it a nice place to work. Their support and friendship made this whole experience really good and helped me to do a better work.

Table of contents

1 Introduction

1.1 The importance of understanding the viscoelastic response of a polymer in elongation

Understanding the viscoelastic properties of polymers has been a subject of great interest for contemporary scientists for many years. Indeed, polymers are now used in almost every field that touches, directly or indirectly, the needs and interests of the population. Whether in the medical industry for the manufacture of prosthetics and medical devices, in the packaging sector to create durable and lightweight materials, or in advanced technologies such as aerospace and electronics, polymers play a crucial role.

Elongational viscoelastic properties, in particular, are especially important. They allows, for example, to optimise manufacturing processes such as extrusion, injection molding and blow molding, ensuring more efficiency and high-quality production. In the extrusion of plastic films, a precise understanding of viscoelasticity allows a precise control of the stretching and thickness of the film, preventing unwanted deformations and structural weaknesses. In injection molding, viscoelastic properties influence the filling of molds and solidification, ensuring defect-free and homogeneous finished materials. For blow molding plastic bottles, viscoelasticity in elongation is essential for achieving uniform material distribution and strong bottle walls.

The role of this master's thesis is, therefore, to focus on the elongational viscoelastic properties of polystyrene samples of various sizes blended together in order to enhance the understanding of the impact of short-chain matrices on the elongational properties of a long linear polymer.

1.2 Objective

The objective of this work aims to understand the role of short chains matrices on the elongational properties of a long linear polymer. This work will also emphasise the importance of determining the glass transition temperature (Tg) as accurately as possible, since, as presented later in this study, this parameter can significantly influence the nonlinear viscoelastic response of the polymer melts and hence, their processability.

The results obtained will be analysed based on the TMA tube model (described in section 2.3 of this work).

To achieve our goal, polymer bidisperse blends composed of a short fraction of long chains (10%wt) blended in short chains of different size have been prepared in order to study the influence of the short chain matrix on the linear and nonlinear viscoelastic properties of the blends. In order to avoid crystallisation issue, the samples studied are based on polystyrene (PS) linear chains. The influence of the short chain matrix on Tg will also be investigated, based on a Differential Scanning Calorimetry (DSC). These samples will then undergo a meticulous analysis of their linear viscoelastic data to obtain master curves of storage and loss moduli as a function of specific frequency

determined experimentally.

Finally, as the viscoelastic response of the long chains are influenced by both the mass of the short chain matrix and the value of Tg, we would like to study the elongational properties of a tridisperse blend, in order to keep the presence of short chains while avoiding a large decrease of the Tg value.

1.3 Outline

This manuscript is organised as follows: First, in Section 2, a state-of-the-art is presented to establish the theoretical and experimental contexts, with a brief explanation of the glass transition temperature and the experimental device used, namely Differential Scanning Calorimetry (DSC), for determining this crucial transition. Additionally, basic concepts of linear and nonlinear viscoelastic properties, as well as the tube model, will be reminded. This section will be concluded with the interpretation of experimental linear and nonlinear data extracted from articles by Shahid et al. and Huang et al., which are valuable for introducing the experimental topics of this work.

Then, in Section 3, the methods employed to prepare the samples, as well as the measurement techniques, will be detailed.

After presenting these theoretical and experimental details, Section 4 focuses on the topic of this master's thesis.

Section 5, which constitutes the biggest part of this master's thesis, discuss in detail the experimental results obtained from the DSC measurements, as well as the linear and nonlinear rheological results for the polymers blends whose composition will be detailed further (see Section 4.1),

Finally, Section 6 offers some conclusions and initiates a discussion on future perspectives.

2 State of the art

In this Section, the basics on the glass transition process are presented, as well as on the rheological properties of a viscoelastic samples. We then present the TMA tube model, which is used later to analyse our data. Finally, we summarise the main results and questions from literature, which are related the elongational properties of linear polymer melts and solutions.

2.1 The glass transition temperature (Tg)

2.1.1 Physical meaning of Tg

The glassy state of a polymer can be described as a state in which cooperative chain motion of the macromolecules are frozen. In this state, only limited local motion can take place, such as side-group rotational/vibrational motions. These motions exist due to bond angle deformation and

bond stretching within the molecules [1]. The glass transition corresponds to the change from this glassy state to a softer and more flexible state at a certain glass transition temperature, Tg, and is characterised by a sudden change in heat capacity and thermal expansion.

The exact description of the molecular motion responsible for the glass transition is not clearly defined, however, it is generally thought to involve macromolecular random chain bond movement, such as groups or segments of the polymer macromolecular relaxing, vibrating or reptating. Above the Tg, the chain segments can undergo cooperative rotational, vibrational, translational, and diffusional motion such that the material is soft and rubbery whereas below the Tg the atoms of polymer chains undergo little rotational-vibrational motions and are in a frozen bulk solid state [1].

2.1.2 The Flory-Fox Iso-Free Volume theory

The Flory-Fox Iso-Free Volume theory postulates that the glass transition occurs when the free or unoccupied volume in the macromolecule reaches a minimum (and constant value) and does not decrease further as the polymer is cooled below the Tg. The free volume (V_f) of the liquid is defined by $V_f = V_T - V_o$, where V_T is the total volume of the liquid at temperature T and V_0 is the theoretical molar volume or occupied volume. The total volume is the sum of the free volume (V_f) and of the occupied volume (V_0). The occupied volume (V_0) includes the van der Waals radii plus the fluctuation volume which is related to the thermal vibrational and rotational motion of the molecule. Thus, the Tg can be viewed as accessing by segmental jumps of the macromolecular chain segments into vacant spaces not occupied by the polymer. The higher the free volume the more easily the jumps can occur and the lower the viscosity and Tg is [1].

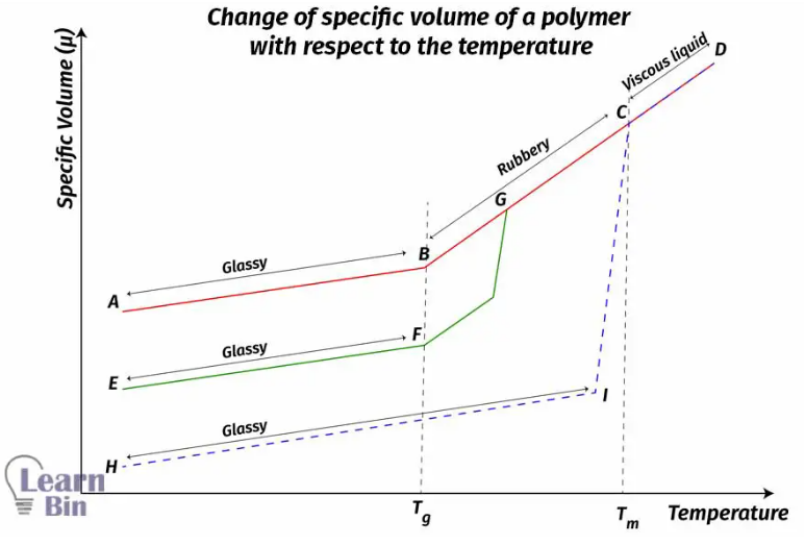

FIGURE 1 – Change of specific volume of a polymer with respect to the temperature for amorphous, semi-crystalline and crystalline polymers[2].

Picture1 illustrates the variation of specific volume for amorphous, semi-crystalline and crystalline polymers with respect to the temperature. The A-D curve represents the thermal evolution of amorphous polymers. Initially, it exhibits the highest proportion of semi-crystalline and crystalline polymers. Between points A and B the polymer exists in a glassy state. With rising temperature, intermolecular forces such as hydrogen bonds and dipole-dipole bonds break, allowing the polymer chains to gain flexibility and begin sliding against each other. Point B corresponds to Tg transition.

As the temperature rises, the polymer undergoes a transition to a rubbery state resembling a viscous liquid (B-C curve). At point C, the polymer has fully transformed into a viscous liquid. At this temperature, the polymer molecules exhibit unrestricted movement within the polymer matrix. The polystyrene used in this work belongs to this first category.

The H-D curve represents the thermal response of a perfectly crystalline polymer, which exhibits no glass transition. Instead, crystalline polymers transition occurs at a certain melting temperature (T_m) directly from a glassy state to a molten state as temperature rises.
Semi-crystalline polymers presents an intermediate behaviour and exhibit both glass transition temperatures and distinct melting temperatures. The E-A curve illustrates the thermal characteristics of a semi-crystalline polymer. The glass transition temperature of semi-crystalline polymers is higher that of amorphous polymers, while their melting temperature is lower than that of crystalline polymers.

Thus, the Tg can be viewed as the temperature at which the macromolecular chain segments can access, though segmental jumps, vacant spaces not occupied by the polymer.

The Temperature coefficient of expansion of free Volume (α_f) is given by the relation

$$\alpha_f(T) = 1/V_g(\frac{dV}{dT}) \tag{1}$$

where V_g is the specific volume at Tg and dV/dT is the observed volume change as a function of temperature. Based with this relationship, the glass transition temperature Tg corresponds to the temperature at which the free volume V_f reaches a constant value. For linear polymers (like the samples considered in this work), the Tg value is an increasing function of the molar mass, such that Tg varies linearly with the reciprocal of the number average molecular weight (M_n). This dependence is a result of the contribution of chain-end segments in molecular motion. As the molar mass decreases, the number of chain-ends increases, and the free volume increases due to an increase of the molecular motions. Therefore the glass transition temperature decreases. This relationship is expressed in the following Flory-Fox empirical equation:

$$Tg = Tg_\infty - \frac{K}{M_n} \tag{2}$$

where Tg_{inf} is the glass transition temperature for an "infinite" molecular weight, M_n is the

number-average molecular weight of the chains (in g/mol) and K is a constant (in °C.Mol/g) determined by the following equation

$$K = 2V_c\rho N_A/\alpha \tag{3}$$

Where V_c is the free volume contributed by chain ends in cm^3, ρ the polymer density (in g/cc), N_A the Avogadro number 6.02310^{23} molecules/mol, and α the thermal expansion coefficient per °Kelvin. Above a certain molecular weight, the influence of M_n on Tg becomes negligible, T_g being well approximated by $Tg = Tg_\infty$.

In case different types of polymer chains are blended, Fox and Flory proposed a relationship, which considers the weight percentage w_i of each type of chains present in the blend and its respective glass transition temperature Tg_i to determine the Tg of the blend:

$$\frac{1}{Tgblend} = \frac{W_1}{Tg_1} + \frac{W_2}{Tg_2} + ... + \frac{W_n}{Tg_n} = \sum_{i=1}^{n} \frac{W_i}{Tg_i} \tag{4}$$

Where Tg_{blend} is the Tg of the blend and w_i/Tg_i is the ratio between the mass fraction of a type of chain divided by its value of Tg. This relationship allows, for example, to determine the glass transition temperature of the bidisperse or tridisperse blends of PS chains considered in this work, from the glass transition temperature of each component.

2.1.3 The main chemical structure factors affecting the value of Tg

Different factors influence the value of Tg, this paragraph lists the main ones:

- The molecular weight for linear homopolymers: an increase in molar mass (molecular weight) leads to a decrease in chain end concentrations, resulting in a decrease of free volume at the end group region and thus leading to an increase the glass transition temperature Tg.
- The presence of diluents or plasticizers: The addition of such compounds increases the free volume and consequently decreases Tg.
- The molecular structure: An insertion of bulky or rigid inflexible side groups (such as a phenyl group, for example) will increase the glass transition temperature Tg due to the decrease in mobility/flexibility, whereas introducing flexible side chains like acetate group decreases Tg.
- The presence of chemical cross-linking: an increase in cross linking density decreases the chain mobility, which leads to a decrease in free volume and thus to an increase of the glass transition temperature Tg. Thus, increasing the branching density increases the free volume, which leads to a decrease of Tg.
- The presence of polar groups: The presence of polar groups increases the dipole-dipole intermolecular forces which increases interchain attraction and cohesion, leading to a decrease in free volume resulting in an increase in Tg.
- The cohesive-Energy Density : An increase of the tacticity decreases Tg whereas an increase of the cohesive energy density increases Tg.

2.1.4 Determination of Tg by differential scanning calorimetry (DSC)

By using the differential scanning calorimetry (DSC) technique, the change in heat capacity of a sample can be measured to determine Tg.

This technique allows determining the temperature and heat flow related to the material transitions, which vary with time and temperature. It quantifies heat exchange either emitted or absorbed by the sample and relative to a temperature difference between the sample and a reference material.

Based on this operational mechanism, DSCs can be categorized into two types: *heat-flux* DSCs and *power-compensated* DSCs. In a heat-flux DSC setup, the sample material is placed in a pan with an empty reference pan, both positioned on a thermoelectric disk surrounded by a furnace. The furnace is heated at a constant rate, and the heat is conducted to the sample and reference pan through the thermoelectric disk. However, due to the differing heat capacities (C_p) of the sample and reference materials, a temperature gradient arises between the sample and reference pans. This temperature difference is measured by area thermocouples and the resulting heat flow is determined by the thermal equivalent of Ohm's law and converted in Watt.

The graph obtained with DSC measurements is nothing else that the power as a function of temperature variation:

$$q = \frac{\Delta T}{R} \qquad [\frac{^\circ C}{\frac{^\circ C}{W}} = W] \tag{5}$$

where q is the sample heat flow, ΔT is the temperature difference between the sample and the reference and R the thermal resistance of the thermoelectric disc.

In a power-compensated DSC setup, the sample and the reference pans are placed in distinct furnaces, each of them being heated by its own heater. Both the sample and reference are kept at identical temperatures, and any variation in thermal power needed to keep this equilibrium is represented graphically in function of temperature or time.

Figure 2 shows a schematic representation of heat flux DSC device that was used for obtaining DSC measurements of our monodisperse polystyrene samples.

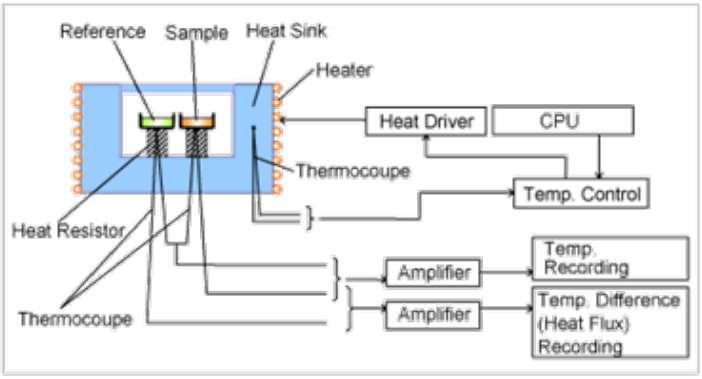

FIGURE 2 – Block diagram of Heat Flux DSC (Hitachi)

2.2 Rheological properties

2.2.1 Linear viscoelastic properties

Measuring the linear viscoelastic properties of a polymer melt or the different blends allows determining their main relaxation times, i.e. the time the chains need to diffuse on a distance of the order of their size, in order to renew their configuration. These characteristic times depends on the nature and the molar mass of the chain, the sample composition and the glass transition temperature of the sample. The determination of the relaxation times of our blends is important to understand their nonlinear properties.

In rheology, the storage modulus G' and loss modulus G" are fundamental functions used to characterise the viscoelastic behaviour of materials. To measure these values, an oscillatory shear deformation is applied to the sample. The more the frequency is large, the less the sample has time to relax, the more it behaves elastically, unable to dissipate energy. On the contrary, at low frequency, the chains, which have time to diffuse and adapt to the deformation applied, behave as a liquid, with no memory of deformation applied. Hence, G" quantifies the energy lost by the material when it undergoes deformation. Materials with values of G" higher than G' exibit more viscous behaviour.

The measurement principle involves an application of a sinusoidal stress or strain to the material at a fixed frequency and amplitude using a rheometer. The amplitude of deformation, γ_0, must be small in order to stay in the linear regime of deformation. The resulting strain or stress response is then measured, allowing the determination of G' and G" values. Stress and strain responses are represented on the figure 3. For an elastic solid, stress and strain are in phase and $\sigma = G\gamma$, and for viscous fluid stress and strain are out of phase, $\sigma = \eta\dot{\gamma}$. For viscoelastic materials, the response involves a combination of both responses, in which the phase angle, delta, depends on the values of storage and loss modulus:

$$\gamma(\omega, t) = \gamma_0 sin(\omega t) \tag{6}$$

$$\sigma(\omega, t) = G'.\gamma_0.sin(\omega t) + G''.\gamma_0.cos(\omega t) \tag{7}$$

and

$$tan(\delta) = \frac{G''}{G'} \tag{8}$$

with ω frequency of the oscillation applied, γ the shear strain, and δ the phase shift angle.

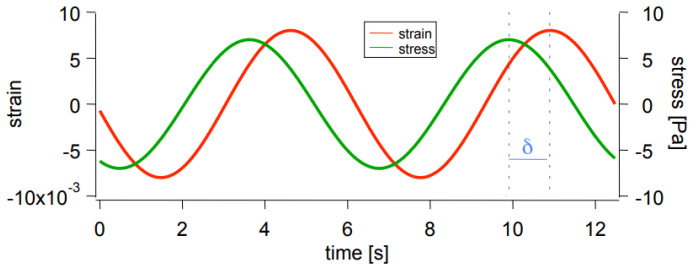

FIGURE 3 – Graphical representation of stress and strain responses as a function of time [3]

Figure 4 illustrates a typical G' and G" master curve as a function of oscillating frequency in the linear domain, in comparison with the relaxation modulus, G(t), which represents the stress relaxation of a viscoelastic material if a constant shear strain is applied, $G(t) = \sigma(t)/\gamma_0$.[3]

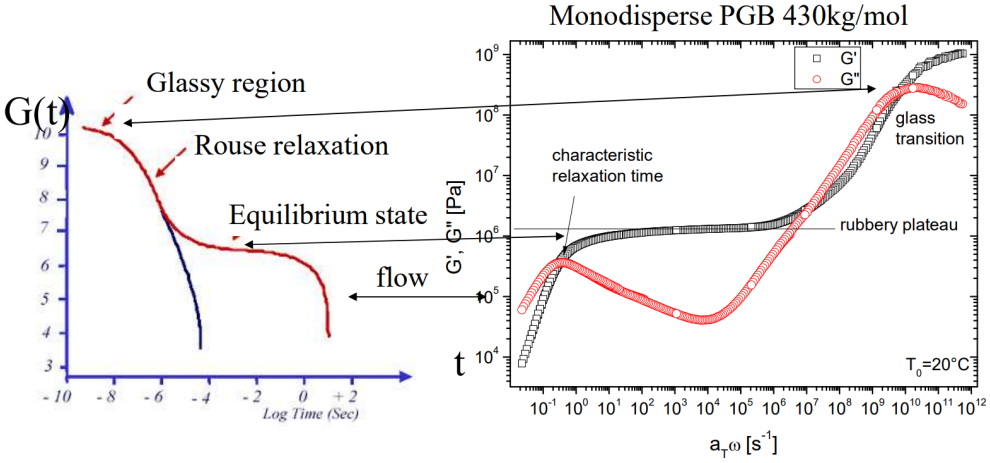

FIGURE 4 – Linear polymer melt: Relaxation modulus G(t) (left) and Typical G' and G" master curves as a function of oscillating frequency in the linear domain (right). The curves arise from for a 430kg/mol monodisperse Polyglycerol butenedioate (PGB). [3]

As the frequency decreases or temperature increases (from right to left), distinct steps are observed in the behaviour of the G' and G" curves:

The glassy region. At high frequencies (or low temperature), G' is very high, indicating that the material behaves like a rigid solid. The polymer chains are immobile and packed, contributing to the material's stiffness. G" is usually lower than G', indicates that while there is some energy dissipation due to internal friction, the elastic behavior dominates. The material exhibits minimal

molecular motion, primarily vibrational.

The Rouse relaxation region. In this region at lower frequencies or temperatures above Tg, G' starts to decrease, indicating that the polymer chains start to move. The polymer undergoes a transition from the glassy to the rubbery state. Small and unentangled chains segments start to relax by Rouse process but the movements of the chains remain limited because they do not have sufficient time and energy to disentangle.

The rubbery plateau region. This plateau represents the rubbery region where the polymer chains have sufficient mobility but are still entangled. G" remains lower than G' in this region. The level of the rubbery plateau directly depends on the density of entanglements.

The flow region. At very low frequencies or high temperatures, G' decreases significantly and the polymer begins to flow, and G" remains constant or increases slightly before decreasing. In this region, the whole chains start diffusing and relax their stress. When the sample is fully relaxed, in the terminal regime, typical slopes of 1 and 2 are observed for G" and G'.

In Figure 4, the transitions between the different regimes are very clear. This is due to the fact that the sample is monodisperse, i.e. all the chains have nearly the same length. Usually, with polydisperse samples, these transitions are less pronounced.

2.2.2 Nonlinear viscoelastic properties under elongation

A. Uniaxial extensional flow In the nonlinear regime, it is common to use a non-dimensional number to characterise the elongation flow imposed to the polymer. This number is the Weissenber number, Wi_R, which is equal $\dot{\epsilon}\tau_R$, the Hencky strain rate multiplied by the Rouse relaxation time of the sample. As described here below, the latter time represents the equilibration time of the sample. For Wi_R larger than 1, the sample does not have time to equilibrate and it is becoming stretched, which leads to strain hardening. On the other hand, at $Wi_R < 1$, the sample has time to equilibrate and no stretch is observed.

Figure 5 shows experimental curves of extensional stress growth coefficient as a function of the time for the PS solutions at 130 °C[4]. The strain hardening curve in the elongational deformation rheology of polymers depicts a typical aspect (see the small representation in the top left corner of Figure 5).

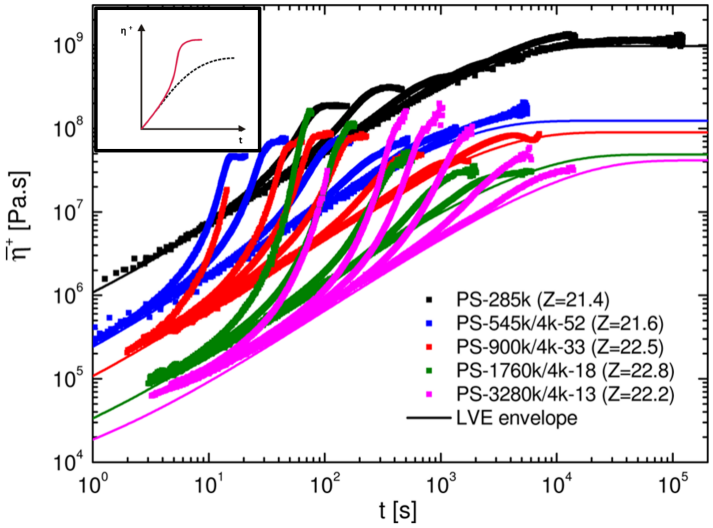

FIGURE 5 – Extensional stress growth coefficient as a function of the time for the PS solutions at 130 °C. [4]

.

Initially, as the material undergoes stretching, the stress experiences rapid escalation. This phenomenon is often attributed to the alignment and straightening of polymer chains in the direction of the applied force. As the strain continues to increase, the stress eventually reaches a maximum point, which indicates a resistance to deformation.
Beyond this point, the material may undergo strain hardening behaviour, characterised by a slight decrease in stress before stabilising or gradually increasing as the strain continues to rise. This behaviour arises from various mechanisms such as chain entanglements, chain alignment, and molecular reorganisation.

Figure 6 illustrates a fluid undergoing uniaxial extensional flow. The sample, initially of length L_0, elongates along the z-axis while contracting along the other two axes to conserve its volume[5].

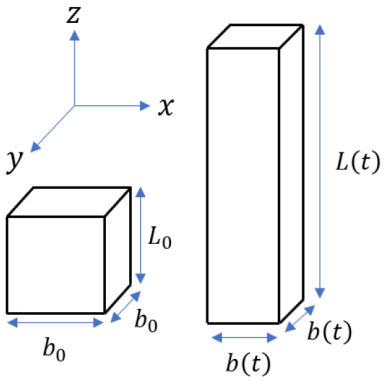

FIGURE 6 – Scheme of a uniaxial extensional flow[5]

.

In the case of an incompressible fluid, the velocity field in an uniaxial extensional flow is described by the following equations[5]:

$$v_x = \frac{-\dot{\epsilon}x}{2} \qquad v_y = \frac{-\dot{\epsilon}y}{2} \qquad v_z = \dot{\epsilon}z \tag{9}$$

In this context, the elongational strain rate is assumed to be constant

$$\dot{\epsilon} = \frac{1}{L}\frac{dL}{dt} \tag{10}$$

where L is the length of the sample at time t.

Integrating Equation 9 shows that the fluid elements separate exponentially over time, and the 3 terms can be reformulated[5]:

$$x(t) = x_0 exp(-\dot{\epsilon}t/2) \qquad y(t) = y_0 exp(-\dot{\epsilon}t/2) \qquad z(t) = z_0 exp(\dot{\epsilon}t) \tag{11}$$

Consequently, uniaxial extension is marked by significant stretching, which orients and elongates polymeric chains. Extensional flow lacks vorticity, resulting in continuous stretching of the chains (see Figure 7)[5].

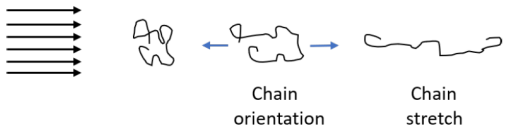

FIGURE 7 – Illustration of polymeric coils under uniaxial extensional flow.[5]

B. The Vader Filament Stretching Rheometer

Nonlinear analysis is carried out by using the Filament Stretching Rheometer (FSR) "VADER-1000" (Versatile Accurate Deformation Extensional Rheometer) described in this section.

In this rheometer, the sample is placed between two stainless steel plates with a diameter of 6 mm. The bottom plate is stationary and connected to the force transducer, while the upper plate is attached to a linear motor for controlled deformations. The sample diameter is monitored by a mobile laser micrometer. The system is embedded in a convection oven, allowing measurements at temperatures up to 250 °C. The device can maintain a continuous flow of inert gas regulated by a flowmeter. This last feature, however, will not be used in the context of our experiments. Figure 8 shows a schematic representation of the filament stretching rheometer VADER 1000[5].

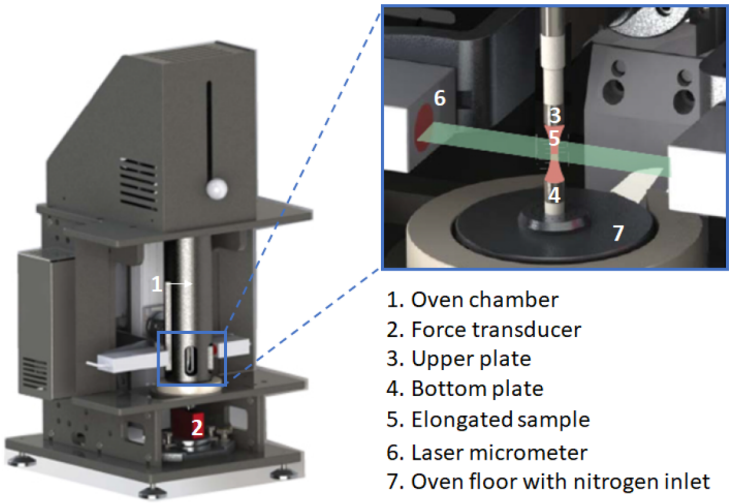

FIGURE 8 – Schematic representation of the filament stretching rheometer VADER 1000. [5]

The VADER 1000 rheometer is equipped with an active feedback control loop, allowing real-time application of the desired kinematic history to the sample, eliminating the need for iterative experimental processes to determine the appropriate plate separation rate. The FSR can conduct various experiments, but only constant strain rate experiments were performed in this work.

In these experiments, the Hencky strain ϵ is obtained using the following relationship [5]

$$\epsilon = -2log\frac{R_{(t)}}{R_{(0)}} = \dot{\epsilon}t \tag{12}$$

where $R(t)$ is the radius at the mid-filament and R_0 is the initial radius of the sample. The control scheme adjusts the upper plate speed to maintain a constant strain rate, while recording the force $F(t)$ exerted by the sample.

Part of the force arises from radial variation due to shear, compensated by a correction factor mentioned by H. K. Rasmussen et al. For larger deformations, this correction becomes negligible, and the extensional stress coefficient $\eta_E^+(t)$ can be calculate by the following equation[5]:

$$\eta_E^+(t) = \frac{F(t) - \frac{mg}{2}}{\pi R(t)^2 \dot{\epsilon}} \frac{1}{1 + \left(\frac{R(t)}{R_0}\right)^{10/3} \exp\left(-\frac{\Lambda_0^3}{3\Lambda_0^2}\right)} \tag{13}$$

In the equation 13, m represents the mass of the sample, g is the gravitational acceleration, and $\Lambda_0 = \frac{L_0}{2R_0}$ the initial aspect ratio of the sample. The second term serves as a correction factor for the shear component. This factor guarantees a deviation of less than 3% from the accurate initial stress if $\Lambda_0 > 0.3$[5].

2.3 Molecular rheological models

Molecular models allow to link the stress applied to the deformation (or vice-versa) of a polymer melt or solution. They can be defined at different length scales. Indeed, three length scales are distinguished: (i) At a very coarse-grained level, the flow properties of the whole polymer sample can be described by constitutive equations. At this scale, which is the order of magnitude used for the constitutive equations, the material appears continuous. (ii) The atomic scale where the system is made of elementary particles, with an order of magnitude of 10^{-10} meters. (iii) The mesoscopic scale, which is an intermediate scale, much smaller than the macroscopic scale and much larger than the atomic scale and the mean free path.

The tube model operate at the mesoscopic scale, for which individual microscopic constituents are not distinguished but only the average effects due to a very large number of particles. This level of observation enables simplification of the model while ensuring a thorough analysis of the system studied.

2.3.1 Introduction

In order to predict the behaviour of non-Newtonian fluids, several models of molecular rheology have been developed. The objective is to establish an expression of the relaxation modulus G(t) as close as possible to the experimental behaviour.For example, the models of Maxwell and Kelvin-Voigt, as well as all models obtained by a combination of elements of Maxwell and Kelvin-Voigt, provide a very good estimate of the relaxation function of viscoelastic materials. Such models have shown to be very efficient to describe the viscoelastic properties of polymer melts. However, this requires accurately defining the model parameters, based on the polymer composition. To this end, different coarse-grained approaches have been proposed, to predict the relaxation time of a polymer chain from its nature, its molar mass, and its molecular environment.

Each molecular models that will be presented here describes a different relaxation process, valid only within a certain window of time and for a specific polymer chain. By combining several models together, we can find an expression for the relaxation modulus G(t) [6].

In these models, at equilibrium and for small strains (i.e. linear regime), G(t) can be interpre-

ted as a measure of how the orientation of each molecular segment correlates with their initial orientation over time. In other words, at the initial moment, the chain has a certain conformation. This chain will be considered as completely relaxed when its conformation has completely changed, which means there is no more correlations with the first one. As the chain relaxes, the stress measured by the rheometer, G(t), decreases.

2.3.2 The mesoscopic coarse-grained model

In this model, some groups of the detailed atomic structure of the polymer chain (yellow beads) are grouped together in a coarse-grained (red) particle. This shows that the detailed information of the chemical structure as well as the degree of freedom of the bond angles are lost. The individual particles are connected by entropic springs (bead-spring model). The semi-flexibility of a large-scale polymer is expressed by the length of persistence[6].

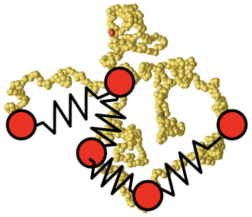

FIGURE 9 – coarse grain representation of a polymer chain

This interpretation leads to a simple chain made up of n Kuhn segments represented by the dumbbells. Kuhn segments are composed of several monomers and have the following characteristics [6]:

— All the Kuhn segments have the same length, noted b.

— The angle between two Kuhn segments can take any value.

— There is no interaction between the Kuhn segments.

The Rouse Model (Rouse, 1953)

This model is generally used to predict the linear rheology of non-entangled molten polymers. It is the simplest molecular model capable of predicting the full spectrum of relaxation of non-entangled flexible chains. The model ignores the hydrodynamic interactions between the beads as well as many other chain effects, which means that it can only be used for non-entangled chains or entangled chains but within a time range limited by the time to balance the stresses of an entanglement strand [7].

In this model, the polymer chains are represented by a system of n beads connected by n-1 springs that follows the Gaussian statistics. Every Kuhn segment has therefore a length b, a friction coefficient ξ_0, and a spring constant $3k_BT/b^2$. The spring is subjected to an entropic force that arises from Brownian motions. Indeed, when a chain is moving, the flow tends to separate the two beads.

The chain is deformed and the number of possible conformations decreases, that leads to a decrease of entropy. Consequently, the chain wants to reduce its end-to-end distance r to minimise the free energy. The expression of the entropic force is the following[6]

$$F_{entropic} = (-3kT/nb^2) * r \tag{14}$$

The beads in Figure 6 represent internal frictions in the polymer chain due to interactions with neighbouring chains or with the solvent. This friction exerts an opposite effect of the entropic force. The friction force is will described by:

$$F_{friction} = n\xi_0 dR/dt \tag{15}$$

with ξ_0 is the friction coefficient for one Kuhn segment. The friction force $F_{friction}$ acts against the entropic force $F_{entropic}$.

For a chain composed of n segments, the total friction for the whole chain is thus:

$$\xi_R = n\xi_0 \tag{16}$$

And the Einstein relationship gives the diffusion coefficient of the chain

$$D = kT/\xi_R \tag{17}$$

When equilibrium is reached, these two forces are equal and cancel each other

$$F_{entropic} = F_{friction}$$
$$(-3kT/nb^2) * r = n\xi_0 dR/dt \tag{18}$$

From this preceding equation, it is possible to obtain a relation for the elongation of the chain over time

$$R(t)/R_0 = exp(-t/\tau_R) \tag{19}$$

with

$$\tau_R = n^2 b^2 \xi_0 / 3kT \tag{20}$$

and τ_R is the Rouse time, that corresponds to the characteristic time needed for an unentangled chain in solution to come back to its equilibrium state.

This simple approach allows determining the characteristic relaxation time of the whole chain. However, in order to accurately describe the chain relaxation, one need to account for its internal relaxation modes. The latter take place at shorter time, and are related to the relaxation of chain segments. As illustrated in Figure 10, this way of conceptualising the polymer chain reveals Rouse modes p, which correspond to the equilibration of chain section containing n/p monomers. Equation 21 gives the relaxation time of a segment p.

The longest relaxation time = $\tau_R \approx \tau_0 n^2$. Furthermore, $\tau_1 \approx \tau_R$ and $\tau_i < \tau_{i-1}$.

$$\tau_p \approx \tau_0 (\frac{n}{p})^2 \tag{21}$$

with n is the number of relaxation modes and p is the number of modes = 1, 2, 3, ..., n. At time $t = \tau_p$, the number of unrelaxed modes = p.

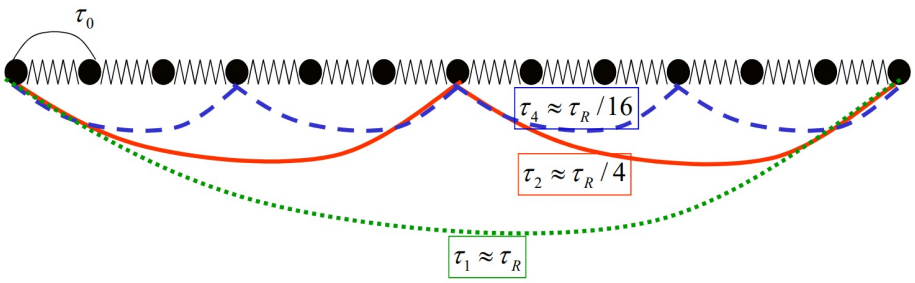

FIGURE 10 – An illustration of Rouse modes on a schematic representation of a polymer chain [3].

The tube model

The tube model has been proposed to explain how an entangled polymer (molten or highly concentrated solution) relaxes the anisotropy and the associated stresses induced by a deformation.

This model reduces the complex dynamics of inter-chain interactions to a simpler process, in which the molecular environment of the observed chain is represented by a tube. In this model, the chain is unable to cross another molecule and behaves as if confined in a tube and for which lateral movements are limited to the tube diameter. Although it depends on the nature and concentration of the polymer, this tube is independent of the architecture of the chains. Moreover, its diameter is constant.

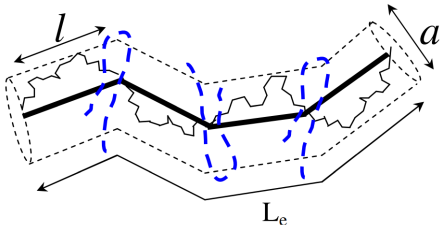

FIGURE 11 – Schematic representation of a tube[8]

The main material parameters of this tube model are the modulus plateau G_N^0, the molecular weight between entanglements M_e which represents the molecular weight of the longest subchain relaxed at this point, and τ_e the Rouse time of a segment between two entanglements. The plateau modulus is directly related to Me, through the following equation:

$$G_N^0 = \frac{4}{5} \frac{\rho RT}{M_e} \tag{22}$$

where ρ is the density of the polymer and T the temperature [8].
The relaxation modulus of an entangled polymer, $G(t)$, can be described by two terms: the first one takes into account the Rouse relaxation of the molecular segment, up to the segments of mass Me. Indeed, the Rouse relaxation of longer subchains cannot occur, due to the confining effect of the tube. The second term describes the tube renewal process proportional to the unrelaxed fraction $F(t)$ of the polymer [8] :

$$G(t) = G_{Rouse}(t) + G_N^0 F(t) \tag{23}$$

This equation is not valid at very short times that correspond to the glassy region because the Rouse modulus diverge at time zero[8]. Different models have been proposed to describe the function $F(t)$. While significant qualitative and quantitative differences are found between the various models, they all use the same mechanisms to describe the relaxation of a chain: reptation, contour length fluctuations and constraint release processes.

Reptation

When the time is larger than the Rouse time τ_e for an entangled segment, the tube picture comes into play: The chain can be seen as a series of tube segments confined by its tube, which represents the surrounding chains. It means that at this time, topological constraints restrict lateral movements of the chain and the chain relaxation can only occur by diffusion according to the axial direction of the tube[8].

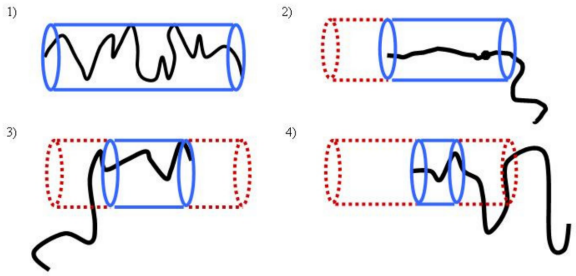

FIGURE 12 – Reptation process[8]

The initial tube is represented in blue (1) and lateral motions of the chain are limited by its wall. When reptation begins, the chain diffuses along the curvilinear axis of the tube and begins to leave it by its ends (2) $\rightarrow$ (4), creating a new tube, the orientation of which is not correlated to the orientation of the initial tube. Consequently, the only part of the chain that contributes to the stress is the one that is still in the initial tube. The chain is considered to be fully relaxed when it has completely left the initial tube.

According to reptation theory, the time τ_{rept} needed to relax the entire chain by reptation is proportional to the cube of the molecular weight of the chain [8]:

$$\tau_{rept} = \frac{L_{eq}^2}{\pi^2 D_c} \propto \frac{M^2}{M^{-1}} = M^3 \tag{24}$$

where the curvilinear diffusion coefficient D_c is equal to $kT/n\xi_0$ and results from the summed drag of all the monomers along the chain. This coefficient is therefore proportional to the number of monomers n and to the monomeric friction coefficient ξ.

The previous relation can thus be reformulated [8]

$$\tau_{rept}(M) = \frac{\xi_0 n_e^2 b^2}{\pi^2 kT}(\frac{M}{M_e})^3 = 3\tau_e Z^3 \tag{25}$$

This M^3 dependence of the reptation time must be compared to the M^2 dependence of the Rouse time.

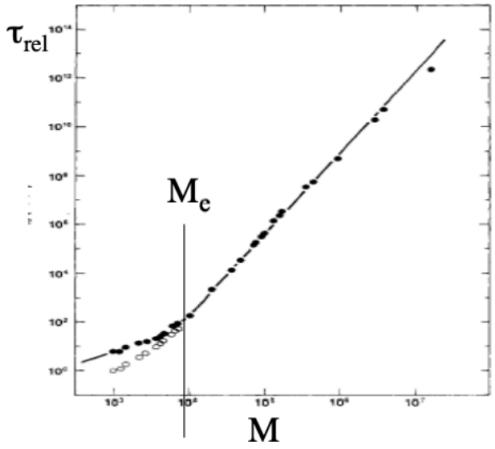

FIGURE 13 – Relaxation times of linear chains in function of their molecular weight M [6]

Figure 13 shows how the relaxation time of a polymer is related to the molar mass. When $M < 2M_e$, the chains are short and untied. In this case the relaxation time is therefore the Rouse time and the slope is equal to 2. Above $2M_e$, the chains are entangled and the relaxation time becomes the crawling time and the slope is equal to 3. In fact, for zero shear viscosity of entangled polymers, the slope displays a value of 3.4, that is slightly higher that predicted by the equation. This slight increase comes from the Contour Length Fluctuations (CLF), which takes place in the relaxation of the chain, thus partially reducing the overall relaxation time. This process will be discussed right after this section.

Reptation is a diffusion process, well described by[8]:

$$\frac{\partial p(x,t)}{\partial t} = D_e \frac{\partial^2 p(x,t)}{\partial x^2} \tag{26}$$

with $D_e = \frac{kT}{\xi_{tot}} = \frac{kT}{n\xi_0}$ the diffusion coefficient, and p(s,t) represents the survival probability of a tube segment s (from 0 at one chain extremity to $L_e q$ at the other extremity) at time t.

By setting the boundary conditions[8]:

$$p(0,t) = p(L_{eq,t}) = 0 \tag{27}$$

$$p(x,0) = 1, \forall x \in (0, L_{eq}) \tag{28}$$

For a segment located at a position x and after a time t the probability relation is the following[8]

$$p(x,t) = \sum_{k_{odd}} \frac{4}{k\pi}.sin(\frac{k\pi x}{L_{eq}}).exp(\frac{-k^2\pi^2 D_t}{L_{eq}^2}) = 1 \tag{29}$$

and by applying this last equation to the whole chain, that is from the beginning to the end of the chain, we obtain the relation for the fraction of the chain that will contribute to the stress[8]:

$$p_{rept}(t) = \int_0^{L_{eq}} p(x,t)dx = \frac{8}{\pi^2} \sum_{kodd} \frac{1}{k^2} exp(\frac{-k^2 D_t}{L_{eq}^2}) \tag{30}$$

Contour Length Fluctuations CLF

This additional relaxation mechanism can be considered as a Rouse relaxation of the chain ends[6], which does not require the motion of the centre of mass as in the pure reptation. The CLF is based on the fact that the length of the chain is not always exactly equal to its equilibrium length, but varies slightly around an average value, L_{eq}. As already mentioned before, a free energy is associated with the chain conformation, and this energy varies with the length of the primitive path of the chain, which is formed by the entanglement segments.

There are two contributions to this potential: the entropic force that tends to bring the two extremities of the chain together in order to increase the number of possible conformations of the chain, and the topological force (from the entanglements) that tends to prevent the chain retraction. It means that the chain is, at any time, in an potential energy state U which depends on the chain length at a certain moment[8].
If now we use the normalised position of a molecular segment, x, which takes values from 0 at the chain extremities to 1 in the middle of the chain, the corresponding potential energy can be written as follows [8]:

$$U(x) = \frac{3kT}{2} Z x^2 + cste \tag{31}$$

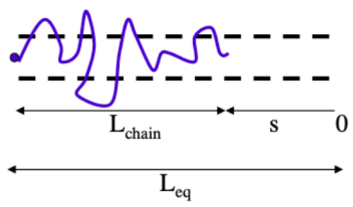

FIGURE 14 – Contour length fluctuation (CLF) process [6]

Two types of fluctuations can be distinguished:

- Early fluctuations

  These fluctuations are due to thermal energy only. The portions of the tube which can relax thanks to early fluctuations are those which are located at a distance x from the end such that the associated potential is lower than the thermal energy[6].

  The value of x satisfies the condition $U(x) < kT$.

  The early relaxation time associated with the onset of fluctuations is defined by the following relation:

$$\tau_{early}(x) = \frac{9\pi^3}{16}.(\frac{M_{arm}}{M_e})^2.\tau_{R,chain}.x^4 \tag{32}$$

- Activated fluctuations

  These fluctuations come from the relaxation by CLF of segments for which the thermal energy is not sufficient to allow the arm retraction on a long distance is entropically unfavorable and is usually not observed for linear chains. Nevertheless, the relaxation mechanism is the main relaxation process of branched polymer melts.

  In this situation, the relaxation time increases exponentially[6]

$$\tau_{activated}(x) = exp(\frac{U(x)}{kT}) \tag{33}$$

  or, equivalently[6]:

$$\frac{\partial ln\tau_{activated}(x)}{\partial x} = 3.\frac{M_{arm}}{M_e}.x \tag{34}$$

  Equation 34 is usually used as it allows accounting for the influence of Constraint Release process via the rescale of M_e (see next section). The value of x for which the fluctuations go switch from early to activated is denoted x_{trans} and $U(x_{trans}) = kT$. The global fluctuation time can be defined as follows[6]:

$$\tau_{fluc}(x) = \tau_{early}(x) \qquad for \quad x < x_{trans} \tag{35}$$

$$\tau_{fluc}(x) = \tau_{early}(x).exp\frac{U(x) - U(x_{trans})}{kT} \qquad for \quad x > x_{trans} \tag{36}$$

  By taking into account these theoretical aspects explained previously, it is possible to formulate the definition of the survival probability by CLF, at a time t and for a segment located at a position x:

$$p_{CLF}(x,t) = exp(\frac{-t}{\tau_{fluc(x)}}) \tag{37}$$

Constraint release process and tube dilation

Dynamic Tube Dilation DTD

The tube represents the topological constraint on a given chain from its molecular environment. It means that the tube itself is able to move according to the movement of the surrounding chains. This movement of the tube, neglected in the model of Doi and Edwards, is particularly important for polydisperse systems. This is particularly complicated to describe in its generality, but fortunately a simplified approach makes it possible to provide a molecular picture that can be resolved more easily.

If the surrounding chains relax faster than the test chain, it means that at time longer than their relaxation time, they are not able to constrain the test chain in its tube anymore. In fact, it these surrounding chains are moving fast enough, once they have relaxed, we can neglect their contribution to the tube and consider that they act as solvent molecules, unable to create effective entanglement. Therefore, the molar mass between two effective entanglements increases and the tube is dilated. This mechanism is called "Dynamic Tube Dilation"[8].

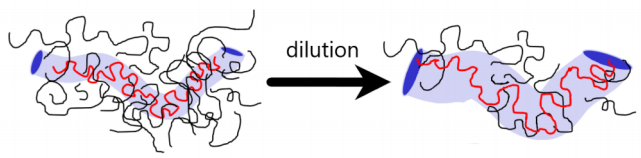

FIGURE 15 – Schematic representation of dynamic tube dilation[9]

This approach is thus based on the concept that the “effective” tube of constraints around a chain widens as relaxation progresses. Given that the surrounding chains are moving continuously, the obstacles disappear and reform, some of them faster near the end of the chain, and the others are slower away from the ends of the chain. If these obstacles had been fixed (i.e. as in the case of a permanent network), the diameter of the tube would have been a well-defined quantity independent of time. Therefore, by considering here the case where the chains are mobile, the segment will be able to move sideways as time passes. This means here that the diameter of the tube should be taken as an increasing function of time during relaxation. For that, it is necessary to consider that the relaxed part of the polymer behaves like a solvent[8].

According to the tube dilution picture, the molar mass between two effective entanglements, $M_e(t)$, the equilibrium length of the dilated tube, $L_eq(t)$ and the effective diameter depend on the unrelaxed fraction of the polymer $\Phi(t)$ according to the relation:

$$M_e(t) = \frac{M_e(0)}{\Phi(t)^{\alpha}} \tag{38}$$

$$L_{eq}(t) = L_{eq}(0) * (\Phi(t))^{\alpha/2} \tag{39}$$

$$a(t) = \frac{a(0)}{(\Phi(t))^{\alpha/2}} \tag{40}$$

By taking the first equation again, it is possible to reformulate the relation of $G(t)$:

$$G(t) = \frac{\rho RT}{M_e(t)^\alpha}\Phi(t) = G_N^0\Phi(t)^{1+\alpha} \tag{41}$$

with α that is called the dilution exponent. It can take a value between 1 and 1.3[8]. In the present work, it has been fixed to 1.

Constraint release Rouse process

Sometimes, the DTD image can lead to a situation where the tube expands too fast compared to the movement of the chain inside the tube. This is particularly true when a small fraction of long chains is diluted in a matrix of short chains, as the blends studied in the present work. If the chains are strongly diluted, the dilated tube can become proportionally very large. Therefore, it is important to add a criterion in any DTD-based model that a chain cannot move into the tube faster than the unconstrained Rouse process.

This mechanism is called the Constraint Release Rouse (CRR) criterion, and can be presented as follows:
In the case of bidisperse polymers where long chains are only lightly or not at all entangled with each other, all entanglements along the probe chains can be considered as short-long entanglements. The entanglement segments have a similar relaxation time, τ_{obs}, which mainly depends on the relaxation time of the shortest chains. In situations where the matrix of short chains is significantly shorter than the long chains present in the blend, Graessley has demonstrated that long chains fully relax more quickly through these constraint release events than by reptation. Therefore, it is assumed that these long chains fully relax via a Rouse process, called the constraint release Rouse (CRR) process [10]. The corresponding terminal relaxation time of the long chains is their CRR time, τ_{CRR},L, which depends on the average waiting time τ_{obs} that takes place on a distance equal to an entanglement segment, and on the number of entanglements along the probe chain Z_L, and is defined by Equation 42.

$$\tau_{CRR,L} = \tau_{obs}Z_L^2 \tag{42}$$

The relaxation time $\tau_{CRR,L}$, is generally larger and never shorter than the intrinsic Rouse time of the long chains, $\tau_{R,L} = \tau_e Z_L^2$, where τ_e is the intrinsic Rouse time of an entanglement segment [10].

Struglinski-Graessley criterion

Even if the chain has sufficient time to explore the enlarged tube in the timescale of its own reptation time, the effect of dynamic dilution is not necessarily felt by the reptation process. This was explained by Struglinsky and Graessley, who found that in a bidisperse mixture of long entangled molecules dispersed in a matrix of short chains, long molecules will reptate in the efficient tube enlarged by the rapid relaxation of short molecules only if their reptation time is sufficiently long compared to their stress release time. This condition accounts for the fact that the short chains

are not a real solvent. The entanglements they create appear and disappear through time, at the rhythm of the motion of these short chains. The long chains can take advantage of this solvent effect only if they had time to explore their dilated tube, i.e. only if their Constraint Release Rouse time is larger than their reptation time in the initial tube.
This is expressed by the following relation:
if

$$\tau_{rept}(M_2) = 3\tau_e Z_2^3 \quad larger\ than \quad \tau_{CRR} = \tau_1 Z_2^2 \quad and \quad (M_2) = \tau_1 Z_2^2 = 3\tau_e Z_1^3 \tag{43}$$

then long chains will relax in the dilated tube[10].

The rheological behaviour of the bidisperse blends used in this work can be explained with the theory described throughout this section. To recap, four bidisperse blends were used, all containing a fixed proportion of 10 wt% of long polystyrene chains with an average molar mass in weight of 820 kg/mol. These bidisperse blends are all composed of short, oligomeric matrix, with a mass of 1400 g/mol (90 wt% PS1k), 2100 g/mol (90 wt% PS2k), 4000 g/mol (90 wt% PS4k), and 8000 g/mol (90 wt% PS9k).

The relaxation of PS820k in the PS1 matrix is expected to be well described by the Rouse model because the very short chains that constitutes this blend behave similarly to a solvent, allowing the long chains to relax more quickly.

For the other blends, the length of the short chains increases, which increasingly contributes to creating entanglements or at least, some friction, that slows down the relaxation of the long chains, with a delay which increases with the molar mass of the short chains. In this configuration, the long chains first relax by Constraint Release Rouse (CRR) process, up to the time at which it reaches its dilated tube (only composed of entanglements between long chains). This process is a Rouse process in which the Rouse time τ_R is replaced by the Constraint Release Rouse time (see Equation 42). Then, at longer time, the tube model well describes the reptation of the long chains. Again, the chains are assumed to relax in a dilated tube (see Equations 38-40), but with a delay compared to relaxation of the same long chains in a real solvent or in the matrix 1k. This delay is accounted for in the reptation and fluctuations process by considering that the relaxation time of an entanglement segment is τ_{obs} (see Equation 39) in place of its intrinsic Rouse time $\tau_{e[10]}$.

The Weissenberg number

The Weissemberg Number (Wi), essential concept within the scope of this work, is a dimensionless quantity used to characterise the extent of deformation or stretching of a polymer melt during processing.

It is named after the German scientist Ernst Weissenberg. The Weissenberg number is defined as the product of the strain rate and the relaxation time of the polymer. Mathematically, it is expressed

as

$$W_i = \dot{\epsilon}\tau_R \tag{44}$$

where W_i is the Weissenberg number, τ_R is the relaxation time of the polymer, and $\dot{\epsilon}$ is the Hencky strain rate.

This dimensionless number helps to indicate whether the deformation of the polymer during processing is dominated by elastic behaviour (high W_i) or viscous behaviour (low W_i). A low Weissenberg number suggests that the polymer has sufficient time to relax and flow, while a high Weissenberg number indicates that the deformation occurs faster than the relaxation rate of the polymer, leading to more elastic behaviour[10].

2.4 Viscoelastic response of a polymer melt under elongational deformation: main questions to address

In the linear regime of deformation (i.e., under small deformation), polymer melts and solutions with the same number of entanglements Z exhibit identical behaviour[11] once the storage and loss moduli of the samples have been normalized by their plateau modulus in the vertical direction and by their entanglement segment Rouse time (τ_e) in the horizontal direction.

Figure 16 illustrates this observation. It is seen that the samples made with polymer melt alone or mixed with oligomers in proportions such that the number of entanglements are displaying the same normalized LVE properties. Figure 17(a) corresponds to the experimental master curves of Figure 16 at 130 °C for different polystyrene solutions, and Figure 17(b) are the normalized LVE data for polystyrene solutions from Figure 17(a)[11].

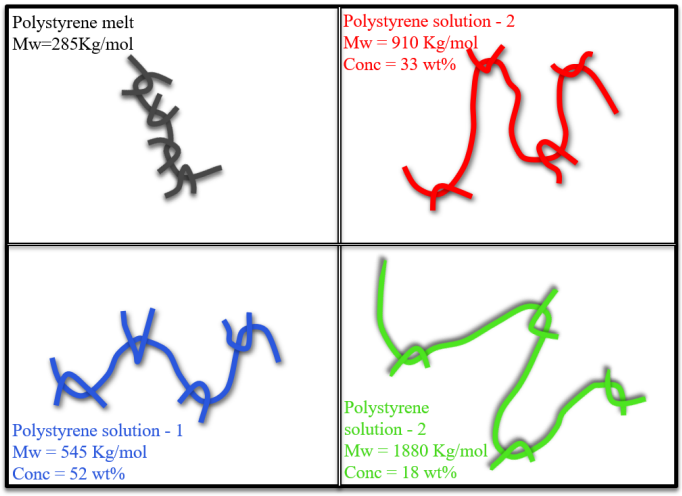

FIGURE 16 – Schematic representation of a polymer melt (PS285k, black) and 3 blends (PS910k/4k 33%wt,red ; PS545k/4k 52% wt,blue ; PS1880k/4k 18% wt,green) with different chain length and different proportion long chain/oligomer but having the same number of entanglements.

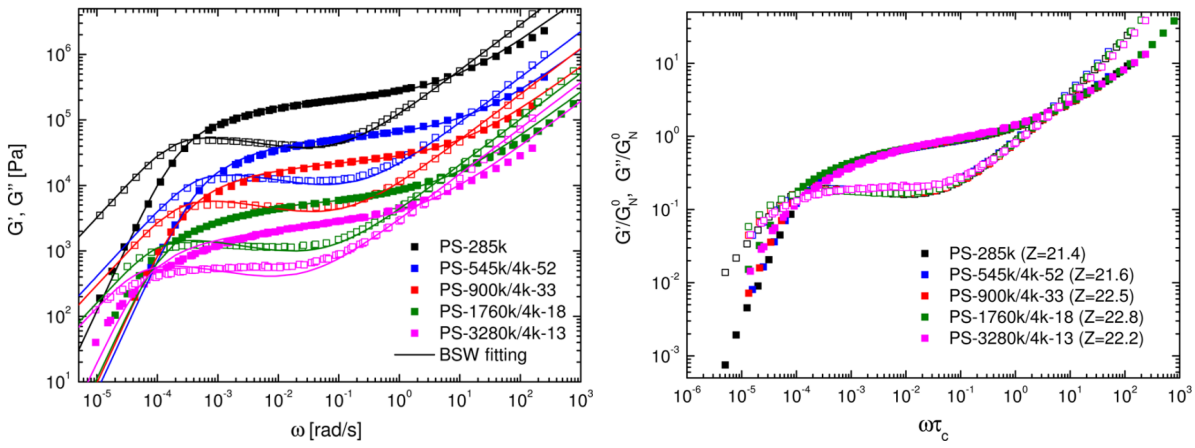

FIGURE 17 – (a) Storage modulus G' and loss modulus G'' as a function of angular frequency ω fitted with the BSW spectrum at 130°C for different polystyrene solutions. (b) Normalized LVE data for polystyrene solutions from (a)[11].

Figure 18 shows the transient viscosity as a function of time for a 40% PS solution of 820k/8.8k (i.e., a sample composed of 40 %wt of polystyrene (PS) with a molar mass of 820 kg/mol, blended to 60 wt% of styrene oligomers of molar mass equal to 8.8 kg/mol). The black solid curve represent the LVE envelope and the blue curves correspond to the viscoelastic response of the sample, which is elongated at a constant Hencky strain rate (see section 5.3).

Each curve corresponds to a different strain rate. Any vertical deviation corresponds to strain

hardening (SH).When the strain rate is relatively low, data more or less overlaps the LVE envelope, however when the stretch rate becomes higher each viscoelastic curve behaves differently. In this figure, strain rate increases from right to left[11].

In Figure 18c, the values of transient viscosity for each steady-state (small red lines on figure 18 (a) and (b)) are plotted in function of deformation rate $\dot{\epsilon}$ (c).

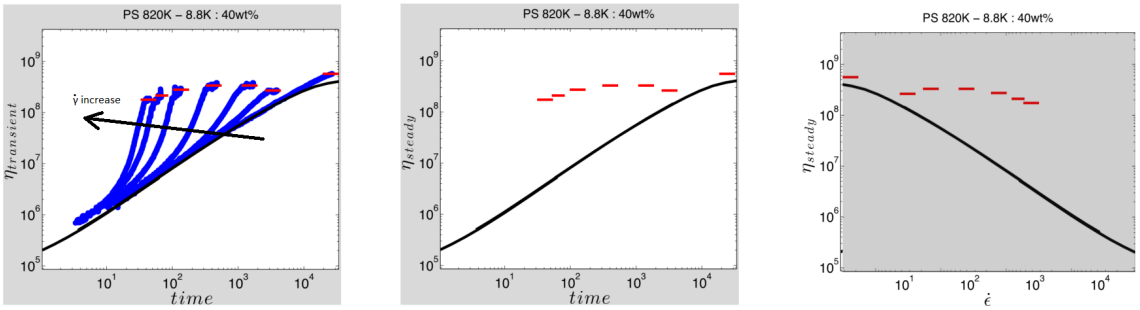

FIGURE 18 – (a) Transient viscosity as a function of time for a 40% PS solution 820k - 8.8k. (b) Isolation of steady-state values. (c) Transient viscosity for each steady-state versus deformation rate.[11]

In ref. [11] ,the steady state viscosity has been determined for all the blends presented in Figure 17. Results are shown in Figure 19. It is observed that the trend of the curves varies from elongation thinning, elongation thinning (blue curve), elongation thinning followed by elongation thickening and again elongation thinning (red curve), to elongation thickening only (green curve). Hence, these different samples are far from showing a universal behaviour, as observed in the linear regime. Today, the origin of this observation is not clear.

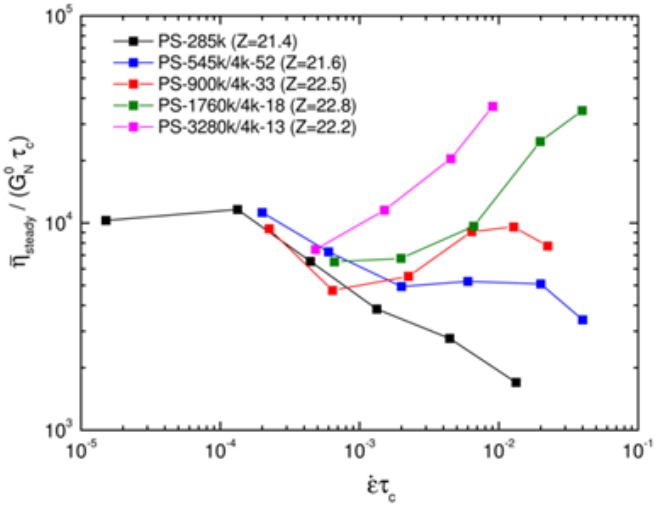

FIGURE 19 – (a) Normalized steady-state viscosity as a function of the normalized stretch rate for the PS solutions.

There would be two key parameters to explain the response in the nonlinear domain:

- o The flexibility of a polymer chain increases with dilution, which means that a polymer can be more stretched when diluted. Hence, the ability of extension thickening also increases.
- o It exists stretch-orientation that induce friction reduction, which promotes strain hardening (SH).

Under large flow, the long chains orient/stretch, which reduces the friction they apply on the test chain, leading to a reduction of the steady viscosity. On the contrary, short molecules do not orient and no reduction of friction is observed, leading to a larger strain hardening effect. This idea has been proposed by Ianniruberto et al [12].

The LVE data measured at different temperatures in Figure 17(a) have been shifted to the reference temperature by using the the time Temperature superposition principle (TTS) to determine the shift factor a_T for each PS solution with the Williams-Landel-Ferry (WLF) equation (see section below).

The Williams-Landel-Ferry equation

To predict the changes in the viscoelastic properties of polymers over time and with temperature variations, the Williams-Landel-Ferry (WLF) equation, proposed by Williams et al. in 1955, is widely used. This empirical equation is indispensable for describing the temperature-dependent viscoelastic properties of polymers in their rubbery state.
Indeed, a similar effect is observed by increasing the observation time or by increasing the temperature, and the relaxation curves at different temperatures are horizontally shifted (along the time axis) according to the temperature shift factor a_T to produce a single master curve.

$$log\ a_T = \frac{-C_1^0 \Delta T_g}{C_2^0 + \Delta T_g} \tag{45}$$

with $\Delta Tg = T - T_{ref}$ corresponds to the difference between the temperature of interest and the glass transition temperature. C1 and C2 are empirical constants specific to the polymer.
The key point is that the constants C1 and C2 are applicable to all samples with different masses under two conditions: (i) the samples are of the same type (polystyrene in this context, and (ii) their reference temperature, T_ref, is chosen such that $(T_{ref} - Tg)$ remains constant.
In addition to look at the steady viscosities, it is interesting to compare the transient response of these bidisperse blends. They are shown in Figure 20, which presents the measured extensional nonlinear data for PS solutions at 130 °C.

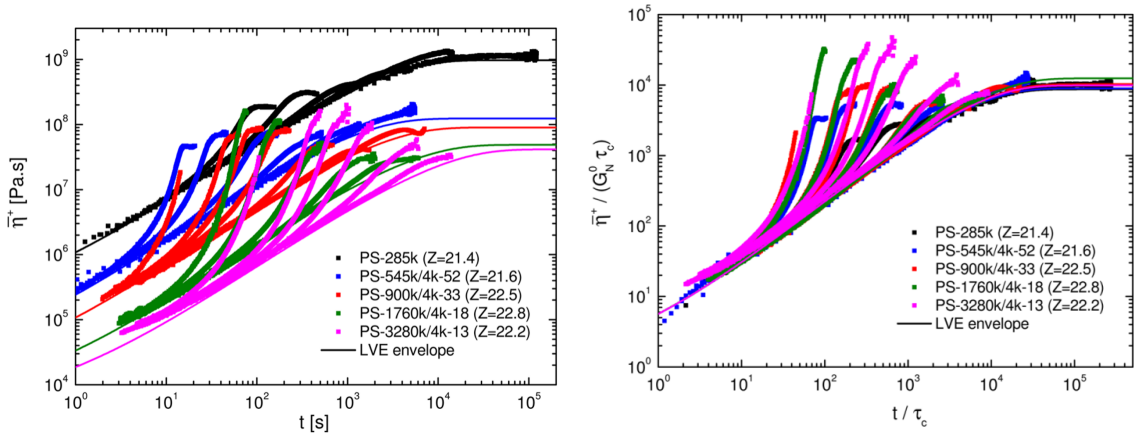

FIGURE 20 – (a) Measured extensional stress growth coefficient as a function of the time for the PS solutions at 130°C. (from left to right): for PS-545k/4k-52: 0.2, 0.1, 0.03, 0.01, 0.003, 0.001 s^{-1} ; for PS-900k/4k-33: 0.2, 0.07, 0.04, 0.02, 0.007, 0.002, 0.0007 s^{-1} ; for PS-1760k/4k-18: 0.06, 0.03, 0.01, 0.003, 0.001 s^{-1} ; for PS-3280k/4k-13: 0.03, 0.01, 0.006, 0.003, 0.001, 0.0003 s^{-1}. Normalized extensional stress growth coefficient as a function of the normalized time for the PS solutions[11].

Figure 20 (a) shows measured extensional stress growth coefficient (or transient viscosities) as a function of the time for the PS solutions at 130°C. Solid lines represent the LVE envelopes. Except for the purple curves that comes from the 3280k/4k solution at the lowest strain rate, η^+ reaches a steady state value. Figure 20 (b) shows normalized extensional stress growth coefficient as a function of the normalized time for the PS solutions. Here again, solid lines represent the LVE envelopes. When the stretch rate is relatively low, data overlap each other for each solution. However, when the stretch rate becomes higher, each solution behaves differently. As it has been shown in Figure 19, the transient strain hardening (and steady viscosity) is more important with increasing the weight fraction of oligomers[11].

In this figure, only the sample PS-285k melt (black curve) has a steady-state viscosity which shows elongation thinning.

This behaviour could well fit the concept of friction reduction (Yaoita and Ianniruberto) since for solutions, the average anisotropy is governed by the solvent and remains small, that doesn't significantly affect the friction On the contrary, for melts, the friction decreases significantly under fast elongation, which leads to a viscosity lower than expected.

To conclude this part, several observations have been made experimentally:

- o PS Solutions that have been normalized, display the same linear properties, but have have different extensional nonlinear properties.
- o For very diluted solutions (< 20% of long chains), there is a systematic change of the exten-

sional steady-state viscosity from stretch rate thinning to stretch rate thickening.

- o The parameters that dominate the nonlinear behaviour wound be the orientation/stretch-induced reduction of friction.
- o Comparison melts/solutions:

  - For solutions (or if concentration decrease), flexibility increases. Friction does not change significantly and global anisotropy is preserved in the oligomers. Stretching increases at higher strain rate, leading to a thickening process.

  - For melts (or if concentration increase), Chain stretching increases, leading to a reduction of friction and consequently, to a steady state viscosity lower than expected. Indeed, elongation thinning is observed.

Influence of the molecular environment[4].

This part discusses the importance of a second key parameter to understand the viscoelastic response of the polymer melts or solutions in the nonlinear domain.

As already mentioned, universality between polymer melts and solutions breaks down under non-linear elongation flows: while polymers melts exhibit a monotonic extension thinning behaviour for all applied strain rates, polymer solutions (with the same number of entanglements) show an initial thinning behaviour followed by extension strain hardening whose effect is amplified when dilution is more important.

In this part, we report the work of Shahid et al., who tested this approach from an experimental point of view based on the extensional response of long polystyrene chains diluted in short chain matrices of different molar masses in order to vary the interactions between long chains and therefore their molecular environment.

According to the friction reduction concept, long chains diluted in a shorter matrix should stretch less. However, in their work, Shahid et al. shows that for a given strain rate, the stretch level reached by the long chains stays the same, whatever the molar mass of the matrix. This result thus questions the validity of the friction reduction.

This is illustrated in the following figures. Figure 21 presents the linear viscoelastic data of a PS820 melt (100 %) and 4 blends prepared with 10 %wt of PS820 and 90 % of respectively PS73 (sample B1), PS34 (B2), PS23 (B3) and OS9 (B4). LVE data at iso-Tg conditions are shown in Figure 21. The "iso-Tg" term refers to the conditions under which comparisons are made at equivalent distance from the glass transition temperature (T-Tg=constant). This is important because the physical properties of polymers, including their mechanical behaviour, can vary significantly with temperature, especially around their Tg. By doing that, the samples are compared at a temperature that reflect the same relative position to their respective Tg.

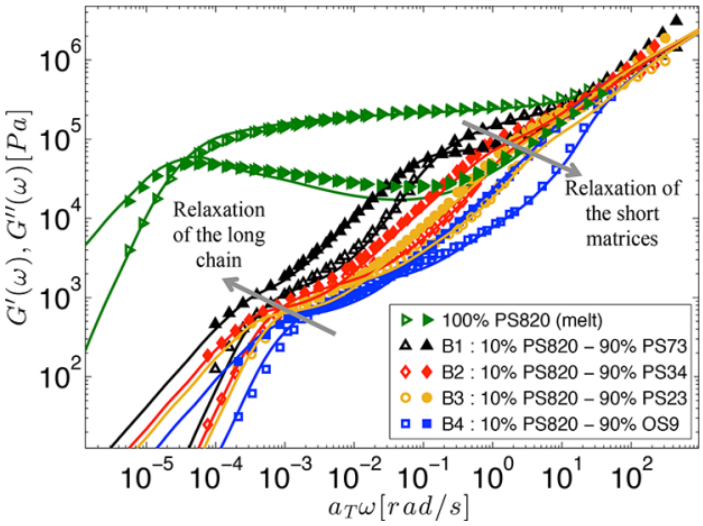

FIGURE 21 – Experimental (symbols) and predicted (lines) storage (open symbols) and loss (closed symbols) moduli of the PS blends at iso-Tg conditions. [4]

We observe that:

- Results show a fast relaxation of the short matrix at high frequencies followed by the relaxation of the long chains at lower frequencies.
- The level of the rubbery plateau and the final relaxation time for melt are higher than for the solutions.
- The width of the rubbery plateau observed for sample B1 gradually diminishes with the size of the matrix molecules, and tends to disappears with the sample B4 constituted with 90% of oligomers.
- The terminal relaxation time also decreases with the size of the matrix molecules, even if the concentration of long chains remains constant. This effect is due to larger constraint release (CR) effect.

These LVE data are used to create the LVE envelope for the elongational data of Figure 22 hereafter.

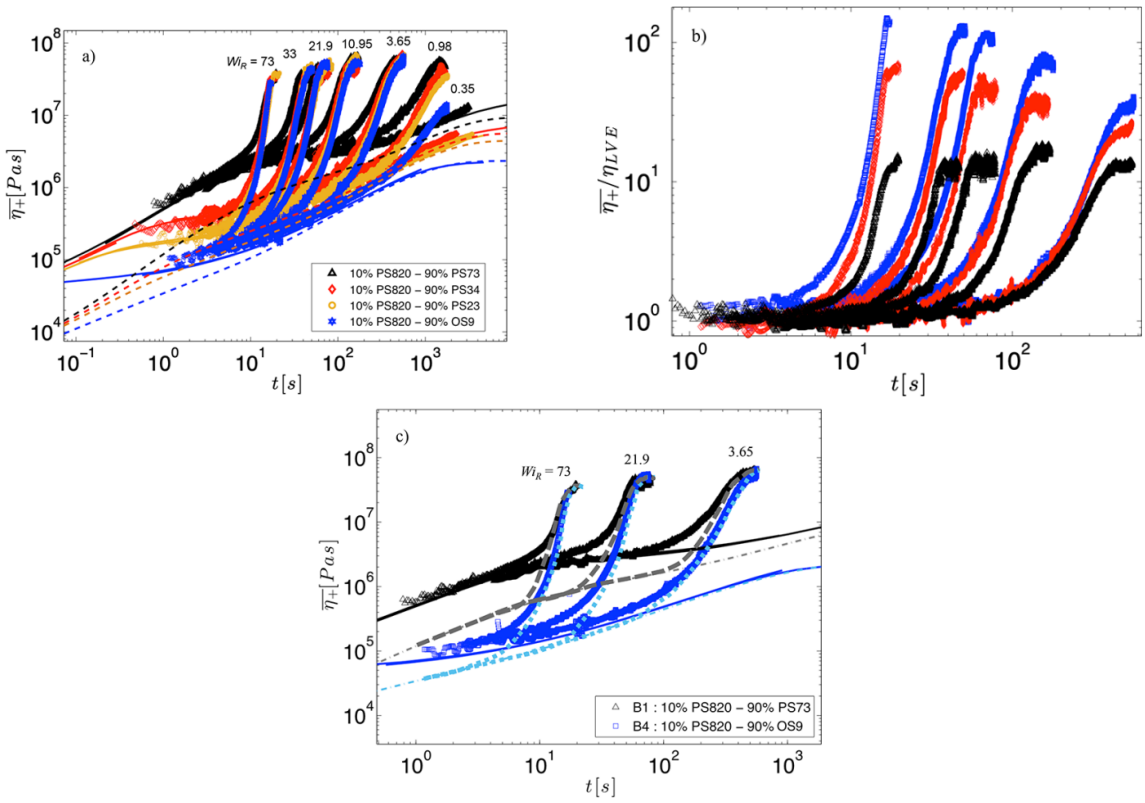

FIGURE 22 – (a) >The transient response of PS blends under elongational flow at various rates as indicated. Solid lines are the LVE envelopes while the dashed lines are predictions of the contribution of long chains to the LVE envelop. (b) Responses of blends B1, B2, and B4 are normalized by the corresponding LVE data in elongation, which have been estimated from the complex viscosity such as $\eta_{LVE}(t) = 3\eta(\omega = 1/t)$ (blend B3 is excluded for clarity). (c) Transient response of blend B1 (black and gray) and blend B4 (blue and light blue) sample. Experimental elongation curves (symbols) are compared to the full LVE envelopes (solid lines) and to the long chain LVE (dash-dotted curves, estimated from model). Dashed curves are drawn to illustrate the onset of long chain stretching. (for clarity, only blends B1 and B4 are shown). [4]

Then, Shahid et al. studied these samples under elongation flow. From the main results, which are presented in Figure 22, several observations can be made:

a) The transient response of PS blends under elongational flow displays an upward deviation, compared to the linear envelope, which corresponds to a transient strain hardening (SH). The latter is attributed to the stretching of the long chains, possibly influenced by the short chain matrix.
It must be noted that during elongation, the Hencky strain rates are low enough to ensure that matrice molecules are not oriented by the flow (the inverse reptation time is shorter than the highest strain rate) and thus, do not contribute to the transient strain hardening.

b) If we look at Figure 22.b, where the data have been normalized by the LVE envelope, we see that

the transient hardening is, indeed, much more important with shorter matrix. However, as shown in Figure 22.c, this is partly due to the fact that the contribution of the short chains to the transient data hides the response of the long chains at short times. These results show that the data based on the ratio shown in Figure 22.b may be misleading.

c) More importantly, it is observed in Figure 22.a that all the PS samples reach the same apparent steady-state value for $W_{iR} = \dot{\epsilon}\tau_{Rouse} > 1$, which means that the choice of the matrix chains has no impact on the final stretch of the long chains.

From this observation, the authors concluded that above a critical molar mass of 4kg/mol, the polymer-matrix interaction has no effect on the long chains stretching. In other words, this shows that, for the different polymer matrices which have been tested, friction reduction does not depend on their molar mass.

An additional comment must be done : Figure 22.a suggests that the long chains reach the same steady-state stretch level and level, but Figure 22.b shows that SH strongly decreases with $M_{w,matrice}$.
As already discussed, this difference comes from the fact that the matrix (when Mw matrix > 4kg/mol) masks initial SH of the long chains. However there is another reason that explains this result. If we observe Figure 22.c, we see that transient SH increases with decreasing the Mw of the matrix as the long chains partially relax by CR process before starting to stretch. This is illustrated in Figure 23. Consequently, long chains diluted in a fast-relaxing matrix partially relax by CR process before starting to stretch.

Consequently and without going into details, the importance of SH increases with the efficiency of the CR process, which means by decreasing the molar mass of the matrix.

We see, in Figure 23, that the viscoelastic properties of the long chains can be divided into two regimes: the first one with (a) and (b), and the second with (c). (a) shows the relaxation state of the chain after this CR process (the chains relaxed from their initial tube represented by the black blobs, to the dilated tube represented by the blue blobs.), (b) represents the chain conformation just before stretching the initial tube (represented by the black blobs). At this stage, SH is already observed. For Figure 23 (c), stretching has started.

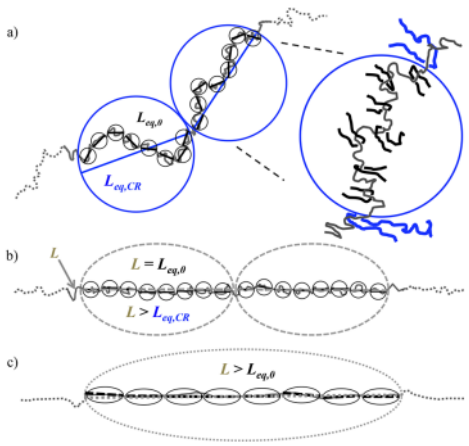

FIGURE 23 – a) Relaxation state reached by the long chain through the CR process. b) Chain conformation corresponding to $L/L_{eq,0} = 1$,that represents the transition state at which $\lambda_{CR} = L/L_{eq,CR} > 1$ while $\lambda = L/L_{eq,0} = 1$. (c) Onset of stretch $\lambda = L/L_{eq,0} > 1$. The grey blobs represent the entanglement segments before the relaxation of the matrix, while the blue blobs represent the dilated tube or the entanglement segments only based on the entanglements between long chains.[4]

Conclusion

- o From this article it results that the role of oligomer size on the strain hardening need to be carefully discussed, as normalisation can lead to wrong conclusions.
- o Above a critical molar mass (of $\approx$ 4 kg/mol for PS) polymer-matrix interactions remain unaltered, and the size of the matrix does not play a role anymore on the final stretching of the long chains, which questions the concept of friction reduction.
- o It exists a clear distinction between transient strain hardening and final stretching of the long chains that determines the steady-state elongational viscosity. The former strongly depends on the polymer matrix, whereas the latter depends on the elongation rate (as well as the long chain Mw and concentration).

It is not clear, however, if these conclusion stay valid if shorter oligomeric matrices are used ($<$ 4kg/mol). Indeed, it has been shown in literature that with short oligomers, possible nematic effects between the long chains and the oligomer could influence the properties as these interactions rigidify the long chains. This question has been partly addressed by Qian Huan in Ref [1]. Results are shown in Figure 25. On the left figure, the experimental LVE data and the data fitted with the BSW model are shown for the solutions of 52% PS 545k in 4k oligomer, 58% PS 545k in 2k oligomer and 52% PS 545k in 1k oligomer measured at 130 °C. Long chains are diluted in same proportion in oligomeric matrices: only Tg is changing, which leads to a horizontal shift of the data. b) shows the shifted data of (a).

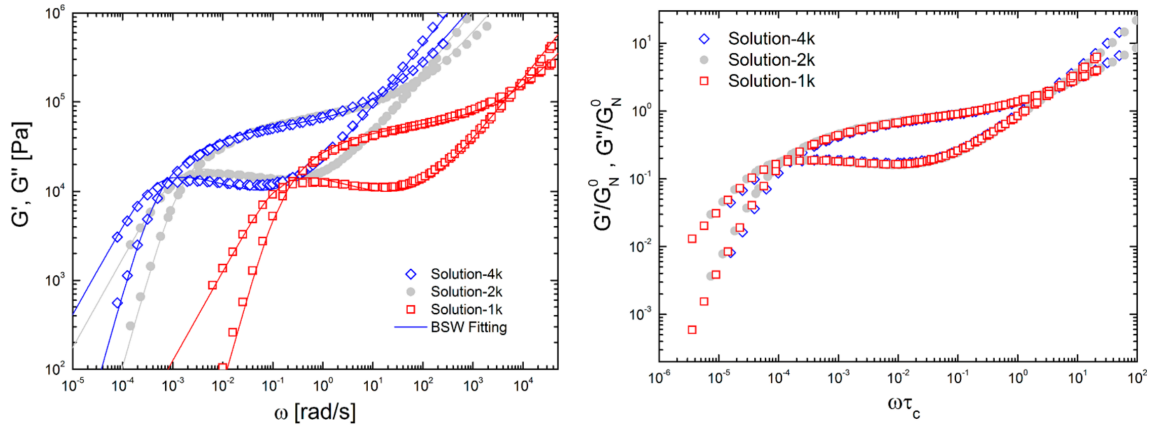

FIGURE 24 – (a) LVE data fitted with the BSW spectrum (solid lines) for solution-4k, solution-2k and solution-1k at 130 °C. (b) Comparison of the LVE data under dimensionless parameters for solution-4k, solution-2k and solution-1k.[1]

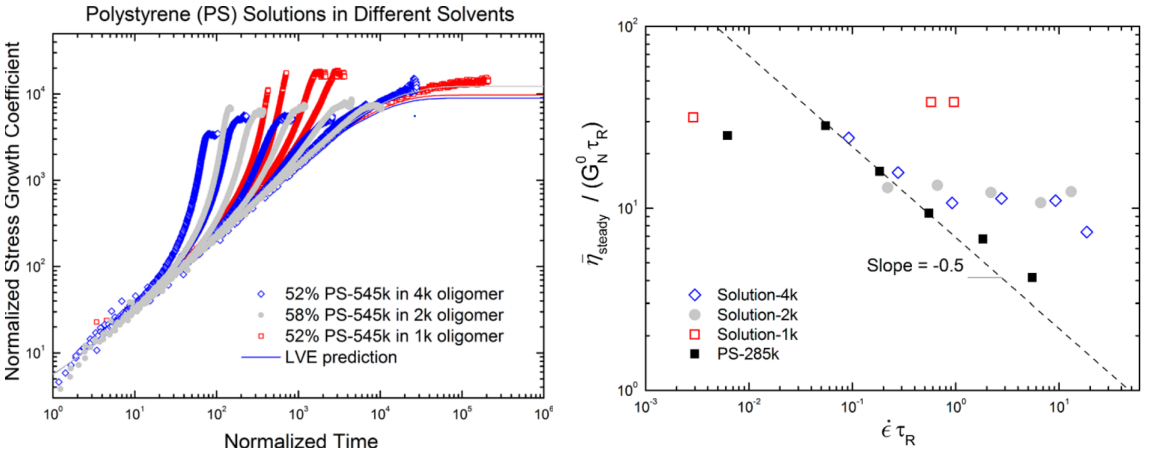

FIGURE 25 – a) Comparison of the normalized extensional stress growth coefficient as a function of the normalised time for Solution-4k, Solution-2k, and Solution-1k in the startup of extensional flow for two concentrated polymer solutions. Weissenberg number ($W_{iR} = \dot{\epsilon}\tau_R$) for Solution-4k (from left to right): 18.5, 9.25, 2.77, 0.925, 0.277, 0.0925 ;W_{iR} for Solution-2k (from left to right): 13.10, 6.69, 2.21, 0.67, 0.22 ; W_{iR} for Solution-1k (from left to right): 3.00, 1.93, 0.965, 0.579, 0.00290. The data for $W_{iR} = 3.00$ and 1.93 were terminated before steady state because of filament rupture. Experiments in the interval 0.579-0.00290 are not shown since the filaments lost symmetry. b) Comparison of the normalized steady-state extensional viscosity as a function of the Weissenberg number for the polystyrene solutions. All the samples have within 12 % the same number of entanglements per chain.[1]

In order to compare the elongational properties of these blends, the latter are deformed at the same Weissenberg number.

In figure 25(a) a large difference is observed in the level of the steady elongational viscosity,

which cannot be explained by the two reasons previously mentioned: It was attributed to nematic effect. However, another explanation could be proposed, based on the large difference observed in the glass transition temperatures of these two blends. Indeed, as shown in Figure 16.a, the use of short oligomers leads to a dynamics which is 1000 times faster for the solution-1k than for the solution-2k. Consequently, the temperature at which these blends have been measured under elongation is largely different. This effect on the data is not clear and have never been investigated.

3 Objective of this Master's thesis

The objective of this Master thesis is to further understanding the role of a short chain matrix on the elongational properties of a long linear polymer. While Shahid et al. have shown that short chain matrix with a molar mass larger than 9k does not affect the strain hardening of the long chains, the influence of an even shorter matrix is not clear, as it was shown here above with the work of Huang et al.

The main difference in the latter case is a strong effect on the Tg of the blend, which can decrease by several decades of degrees. In the present work, we aim to complete the work of Shahid et al., based on the same long chains (PS820k), diluted in the matrix at the same proportion (10 wt%), and explore the influence of shorter matrices. This requires, first, to analyse the effect of these short matrices on the glass transition temperature of the blends, via DSC technique, Fox-Flory model, or rheology. Then, it requires an accurate analysis of their linear viscoelastic data and on the construction of their master curves. Since the latter are strongly dependent on the choice of Tg, a good overlap of the data is an additional way to validate the value determined for Tg. The master curves obtained are also modelled, based on the TMA tube model (see Section 5.2), in order to further check their consistency.

Finally, the elongation properties of the blends are studied. A specificity in this project is to consider a tridisperse blend, in addition to the more classical bidisperse blends. This allows us to vary the Tg of the blend, independently of the influence of the relaxation time of the short chain matrix. Hence, it gives us additional information on the influence of the short chain matrix on the strain hardening properties of the long chains.

4 Materials and methods

The material used in this work is polystyrene (PS) in the form of monodisperse samples of different molecular weights, and synthesised by anionic polymerisation.

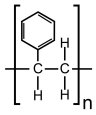

FIGURE 26 – Molecular structure of polystyrene molecule

4.1 Samples preparation

4.1.1 Preparation of bidisperse and tridisperse samples

Monodisperse polystyrene samples (referred as "short chains" in this work) are used to prepare the bi and tridisperse blends needed for the measurements. Bidisperse blends are made by mixing PS oligomers with polystyrene 820 kg/mol (referred as "long chains"). The weight ratio is fixed to 90 % of short chains for 10 % of long chains, and the blends are prepared according to the following procedure:

a. The first step involves weighting each monodisperse sample to obtain an overall mixture containing 10% of long chains (i.e. the 820k sample).

b. The monodisperse samples are then dissolved in tetrahydrofuran (THF) and the solution is kept under agitation until complete dissolution of PS samples. The solvent is then evaporated under chemical hood.

c. When the solvent is nearly completely evaporated, the preparation is placed for 72 hours at 50°C in an oven under vacuum, that is a minimum duration to ensure that there is no more solvent in the PS sample. Indeed, some residual amounts of solvent would modify the results obtained with DSC measurements, which is the next step after preparing the samples.

Table 1 summarises the different polystyrene samples and polystyrene blends used throughout this work as well as the composition of the blends. The arbitrary designation of the samples and the blends presented in this table will be used throughout this document.

Polystyrene samples		Blends	
Name	Mw (g/mol)	Name	Composition
PS820k	820 000	BIDISPERSE	
PS34k	34000	90%wt PS9k	90%wt PS9k / 10%wt PS820k
PS9k	8800	90% wt PS4k	90% wt PS4k / 10%wt PS820k
PS4k	4000	90% wt PS2k	90% wt PS2k / 10%wt PS820k
PS2k	2100	90% wt PS1k	90% wt PS1k / 10%wt PS820k
PS1k	1400	TRIDISPERSE	
		Tridisperse	33,5%wt PS4k / 56,5%wt PS34k / 10%wt PS820k

TABLE 1 – Summary of theoretical and experimental Tg values for monodisperse samples and for blends used in this work.

4.1.2 Preparation of the polymer disc

The next step is the preparation of the cylindrical polymer sample that will be inserted into the rheometer. For more clarity, this cylindrical polymer sample will be named polymer "Disc" throughout the work. It is important to note that due to the difference in plate dimensions depending of the rheometer used, two different disc size are used: linear measurements with PAAR and ARES rheometers require a disc of diameter of 8mm whereas nonlinear measurements with VADER require a disc of diameter 6mm.

preparation of the 8mm disc

a. In order to perform rheology tests, the samples must be shaped into small discs of diameter of 8mm and thickness of around 0.7mm. To this end, a mass of 40 mg of polymer blend previously dried in the oven is measured by using a precision balance before being inserted into the appropriate 8 mm mold. This latter is then closed and locked with the appropriate screws, and vacuum is applied by using a vacuum pump. The latter will be be maintained throughout the disc preparation to ensure that there is no air bubbles trapped into the final solid sample.

b. The mold is then the heated at a temperature that depends on the glass temperature of the blend. Usually, the temperature applied is approximately equal to Tg + 40°C. The sample heating is maintained for 20 minutes to be sure that the dry quantity of powder is completely molten.

c. After this time, a weight is placed on the mold cover whose axis is in contact with the sample in order to apply a pressure that will agglomerate the melt polymer and give it the desired cylindrical shape. Heating is maintained 15 minutes in this configuration.

d. Finally, heating is turned off and the mold is removed from any heat source, but vacuum is still applied. After 20 minutes of cooling, the sample is ready to be removed. The mold is cautiously opened and the appearance of the disc is checked. The sample is considered valid if the disc is homogeneous, clean, and free from any cracks.

preparation of the 6mm disc

In order to perform nonlinear elongational measurements, discs of 6 mm diameter must be prepared. The steps are mainly identical to the 8 mm disc, however it must be noted that it is very important not to exceed 50 mg of material because an excess of mass will lead to increase the quantity of polymer which will be stretched in the elongation rheometer. In such a case, it is probable that the maximum deformation that the rheometer can apply (of around 700%) does not suffice to reach the steady state of the sample deformed a constant strain rate. For this reason, it is required not to exceed a weight of 40 mg. A value of 35mg seems even more suitable for the disc intended for nonlinear analysis.

4.1.3 Measurements protocol

Anton Paar and ARES rheometers

Rheological experiments in the linear domain are performed with the Anton Paar MCR301 and with the Advanced Rheometric Expansion System (ARES), both equipped with an 8 mm diameter disc in plate-plate geometry configuration. The usage is similar for both rheometers, and for this reason, the procedure will be explained only once for both models.

o Sample Loading

Before loading the sample disc, the equipment must be cautiously cleaned with a small amount of acetone impregnated on absorbent paper, for example, to ensure accurate and reliable results. The temperature is then set to the desired highest temperature for the initial experiment. The zero fixture is performed at this specific temperature. The sample is loaded afterwards. It is necessary to allow the material to relax for approximately 15 minutes. This time is certainly not a constant and varies depending on the polymer used. it should be noted that the experiment temperature is obviously above the Tg of the material.

o Dynamic Strain Sweep Experiment

In a dynamic strain sweep experiment, the sample is subjected to a sinusoidal strain wave at a constant frequency of oscillation, but with varying amplitudes $\gamma 0$, and the resulting stress is measured. This technique allows to establish the limit of the linear regime of deformation for the material. The experiment is conducted at the highest available frequency of 100 rad/s, for strains ranging from 0.1% to 100%. It is important to mention that the test is interrupted as soon as a slight decrease in the storage modulus is observed, in order to avoid entering the non-linear regime. Additionally, this technique ensures that the sample is properly fixed in the rheometer. If noise is observed instead of a plateau for small strain amplitudes, it might indicate that there is a poor contact between the sample and the parallel plates or that the transducer used is not appropriate. This problem can be resolved by reducing the gap or by changing the transducer type.

o Dynamic frequency sweep

This method is employed to determine the storage and loss moduli of the investigated materials. The frequency range spans from 100 rad/s to 0.01 rad/s. this test has been carried out for different

temperatures, from the highest temperature the sample can reach before loosing his properties due to thermal degradation, to the lowest temperature for which the properties of the sample are still measurable, which is less and less the case when approaching the Tg of the sample.

To prevent any damage to the rheometer, it is important to be careful when unloading the sample. The unloading process should be carried out at a sufficiently high temperature to allow the material to flow and not restrict the transducer. This approach ensures that the sample can be removed without applying excessive axial forces on the transducer while separating the parallel plates.

VADER rheometer

Measuring the elongational properties of a sample is rather tricky, as the sample can easily detached or deform in an inhomogeneous way. Therefore, it was important to settle a clear protocol of measurement. The latter is defined here:

a. Starting the rheometer and sample loading
   To begin, press the button ON/OFF on the left side of the rheometer and start the COMPASS® program. Open the chamber and verify that the plates are clean. If there are not, cautiously clean them with a small amount of acetone impregnated on absorbent paper. Once this is done, enter into the "force and gap setting" menu, choose the force of the transducer and click on the "zero gap" button. This step is crucial because the zero-gap will fix the reference in terms of plate position, and therefore influence the value of upcoming experiments. Then, press on "tare" to reset the measured force, which will be equal to zero since there is actually no charge on the plates. Place the disc sample on the lower plate, close the chamber, set temperature on the desired value and click on the "ON" button.

b. prestretching
   When the sample is inserted in the oven and the temperature is rising, the height and the diameter of the disc is measured by using the laser measurement and entered into the experimental parameters in the COMPASS® program simultaneously with experimental parameters and the desired Hencky strain rate. As the temperature increases beyond the Tg, the sample will start to deform and present a rounded shape. At this moment, one needs to push on "tare" for the last time and move the top plate closer to the sample until there is a contact. This can be observed by looking after the force measurement that becomes negative after the contact. Indeed, Negative value are due to the conception of the rheometer that measure a positive force when the sample is stretched.
   Once the contact is established, a waiting time of about 10 minutes is necessary to ensure a correct adhesion between the upper plate and the sample. After this time, prestretching is started in order to decrease the disc diameter to a value close to 3,4 mm. A waiting time is again necessary so that the residual force becomes lower than 0,1 g, which means that the polymer is relaxed and ready for measurement. The diameter and the hourglass shape of the filament is checked (by clicking on "Scan Filament").

c. Nonlinear analysis

Once the sample is relaxed and the appearance of the filament is checked for the last time and the elongational test is started. The force and the filament diameter are recorded all long the experiment. The end of the measurement is indicated if the filament breaks or if the amplitude of deformation reached his maximum value. This last condition means that the filament is still fixed by its two extremities when the upper plate reached its maximum upper position.

d. Sample retrieving and machine shutdown

When the measurement is done, a particular attention is dedicated to sample removing to avoid imposing too much force on the transducer. For doing that, the sample temperature must be sufficiently high, which means that it should not be below the prestretch temperature.

5 Results

5.1 DSC analysis

5.1.1 Determination of the glass transition temperature of the PS samples

This section of the work will be dedicated to discuss the experimental results obtained with the DSC.

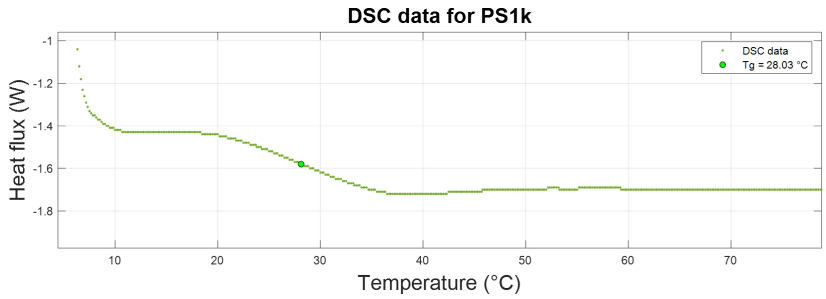

FIGURE 27 – Determination of Tg by DSC for the 1k PS sample.

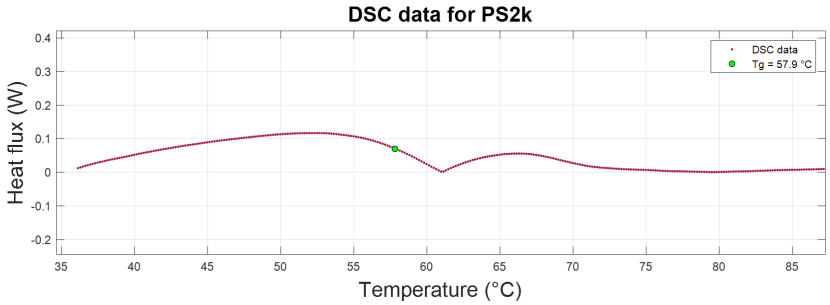

FIGURE 28 – Determination of Tg by DSC for the 2k PS sample.

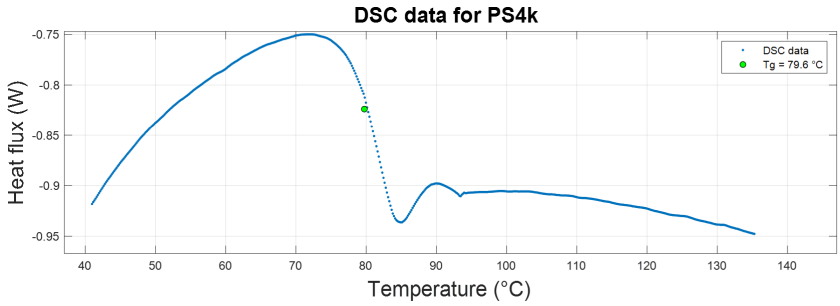

FIGURE 29 – Determination of Tg by DSC for the 4k PS sample.

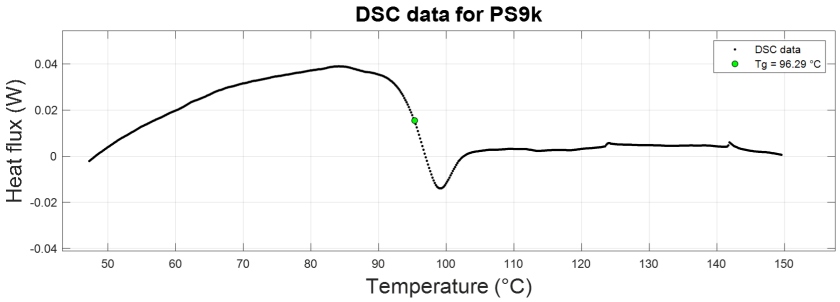

FIGURE 30 – Determination of Tg by DSC for the 9k PS sample.

and the curves corresponding to DSC measurements of bidisperse and tridisperse polystyrene blends are shown below.

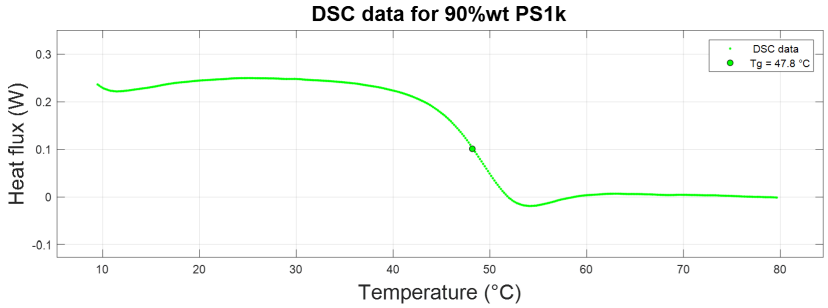

FIGURE 31 – Determination of Tg by DSC for the 90%wt 1k PS blend.

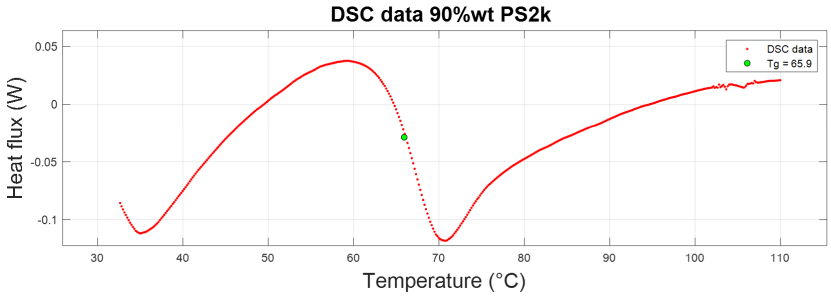

FIGURE 32 – Determination of Tg by DSC for the 90%wt 2k PS blend.

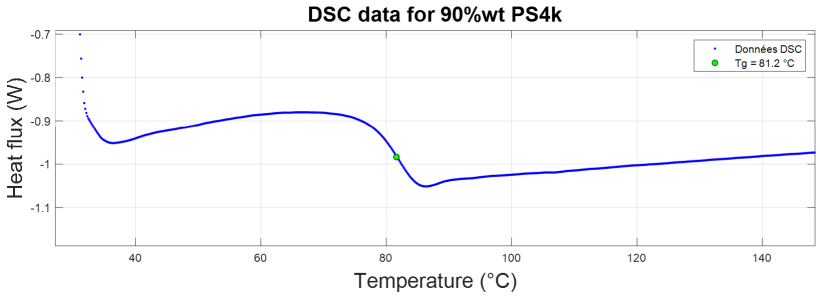

FIGURE 33 – Determination of Tg by DSC for the 90%wt 4k PS blend.

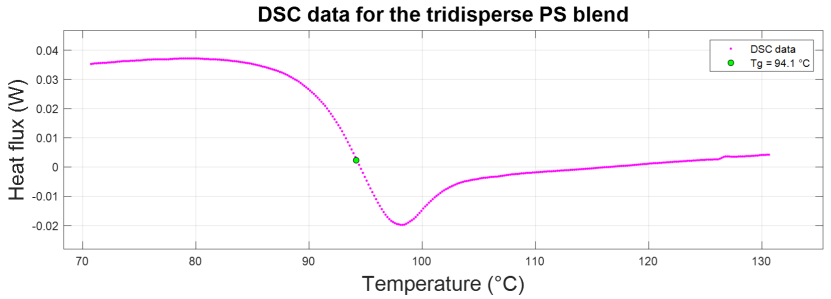

FIGURE 34 – Determination of Tg by DSC for the tridisperse PS blend.

Polystyrene samples				Blends			
Name	**Mw (g/mol)**	**Theory (°C)**	**DSC (°C)**	**Name**	**Composition**	**Theory (°C)**	**DSC (°C)**
PS820k	**820 000**	106,47	N/A	BIDISPERSE			*data from Shahid et al.
PS34k	**34000**	103,36	N/A	**90%wt PS9k**	**90%wt PS9k / 10%wt PS820k**	95,77	98,6*
PS9k	**8800**	94,1	96,29	**90% wt PS4k**	**90% wt PS4k / 10%wt PS820k**	81,67	81,21
PS4k	**4000**	79,1	79,61	**90% wt PS2k**	**90% wt PS2k / 10%wt PS820k**	58,79	65,92
PS2k	**2100**	54,22	57,93	**90% wt PS1k**	**90% wt PS1k / 10%wt PS820k**	34,39	47,79
PS1k	**1400**	28,03	27,91	TRIDISPERSE			
				Tridisperse	**56,5%wt PS34k / 33,5%wt PS4k / 10%wt PS820k**	95,75	94,2

TABLE 2 – Summary of theoretical and experimental Tg values for monodisperse samples and for blends used in this work.

The Tg data of the monodisperse samples are then plotted in Figure 35, as a function of their molar mass, together with different sets of data found in literature. This allows us to determine the parameters of the Fox-Flory equation (see Equation 2), based on a (Nelder-Mead) minimization algorithm of Matlab, which is a multidimensional unconstrained nonlinear minimization function. According to this equation, the values of the glass transition of our monodisperse polystyrene samples of 820k - 34k - 8,8k and 4k should be respectively 105,5 - 102,2 - 95,3 and 83,1 °C. These values must be compared to the values found by DSC, which are given in Table 2. A good agreement is observed for PS samples of 4k and 1.4k, while a non-negligible difference of 3.7°C is found between the theoretical and the measured Tgs for PS samples of 2.1k.

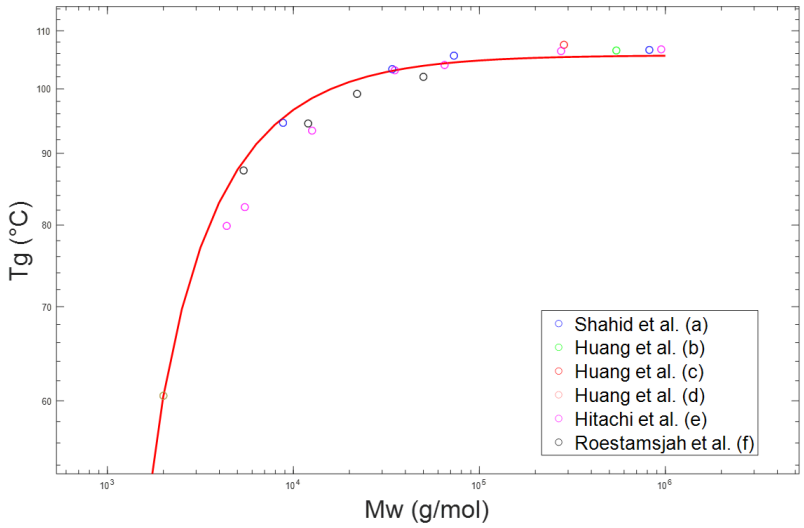

FIGURE 35 – The glass transition temperature of samples derived from the literature (a:[4], b:[13], c:[14], d:[15], e:[16], f:[17]) as a function of their molecular weight. The red curve corresponds to the modelization based on a (Nelder-Mead) minimization algorithm.

In addition, the theoretical values of Tg determined from the Fox-Flory relationship for polymer blends are also determined, based on the theoretical Tg of the monodisperse samples. Their values are compared to the experimental data in Table 2. Large discrepancies are observed between the theoretical and the experimental data for the blends containing the PS sample 2.1k (around 7°C) as well as for the blend containing the PS sample 1.4k (around 13°C), while a good agreement is found for the blend containing the PS sample 4k. The origin of this difference is not clear. For the 2.1k sample, it is observed that the experimental value of Tg is better approximated by the Fox-Flory relationship if we consider the experimentally determined Tg of the monodisperse PS 2.1k rather than its theoretical value. However, for the 1.4k blend, nearly no difference observed between these two approaches. As shown in Figure 35, the dependence of Tg on the short chain matrix is very large. Therefore, a small variation can easily lead to few degrees difference in Tg.

Furthermore, Figure 35 shows that Tg increases rapidly with molecular weight. This is due to

the reduction of the mobility of the individual chain segments. Short chains are less constrained and more mobile, resulting in a lower Tg. As the molecular weight increases, the interactions between the chains become more significant, thereby increasing Tg.

As shown in this figure, the section of the Tg versus molecular weight curve between 1000 and 10000 g/mol has the steepest slope. This indicates that an imprecision in the measurements for low molecular weights has a more significant impact than for higher molecular weights.

Additionally, the tridisperse polystyrene blend must contain short oligomers (1k) but should have a relatively high Tg. For this reason, a fraction of 34k has been added to achieve the theoretical Tg of the 9k bidisperse blend. The experimental value is 94.2°C, which is close to the theoretical value of 95.75°C.

5.2 Analysis of the linear viscoelastic properties

As it is important to determine their glass transition as accurately as possible for understanding their viscoelastic response, a third technique has been used, based on the rheological data. It consists of measuring the linear viscoelastic data of each blend at different temperature and build the corresponding master curve, by horizontally shifting the data on a reference curve.
According to the literature, if the reference temperatures $T_{ref,1k}$, $T_{ref,2k}$ and $T_{ref,4k}$ are selected in order to ensure that the difference between each of these reference temperatures and the corresponding glass transition temperature of the blends, T_{1k}, T_{2k} and T_{4k}, is equal (i.e. $T_{ref,i} - Tg_{,i}$=constant), their high frequency response, which reflects the chain dynamics at very short length scales, would superimpose. Equivalently, if we find a reference temperature for each of these blends such that all the data superimpose at high frequency, this means that reference temperatures have been correctly chosen.

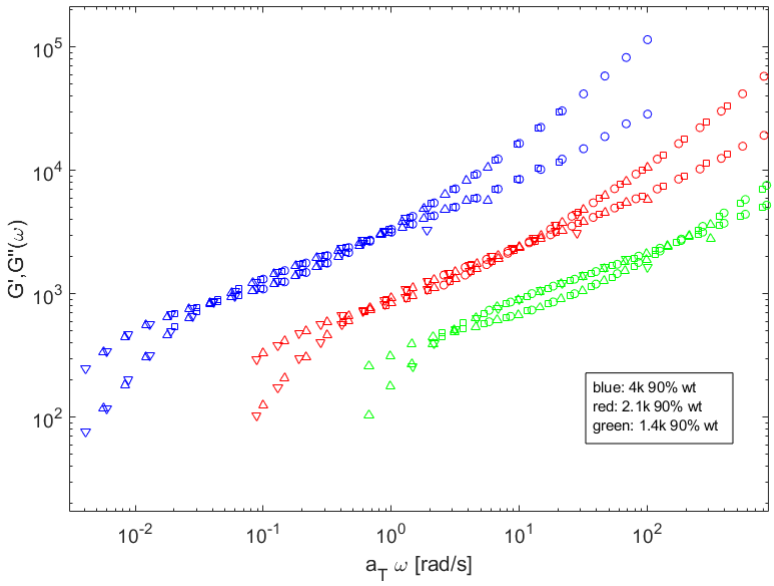

FIGURE 36 – Master curves of G' and G'' as a function of oscillation frequencies for the bidisperse blends 4k, 2.1k and 1.4k, at a reference temperature of 125°C

Figure 37 shows the experimental data, plotted at a reference temperature of 125°C, which is common for the three blends. This means that the data at 125°C are not shifted, while the storage and loss moduli measured at another temperature have been manually shifted in order to well superimpose on these reference curves.
The corresponding master curves obtained for the storage and loss moduli of the three bidisperse blends show a good overlap of the data. However, as expected, these master curves clearly do not superimpose at high frequency, highlighting the fact that these samples do not have the same Tg.

It is also instructive to plot the phase angle δ in function of the frequency for these three blends, as this value is more sensitive to small discrepancies in the shift factors. Results are shown in Figure 37. A good overlap of the shifted data is also observed. Moreover, it is seen that at low frequency, the phase angle approaches a value of 90°, i.e. behaves as a viscous sample.

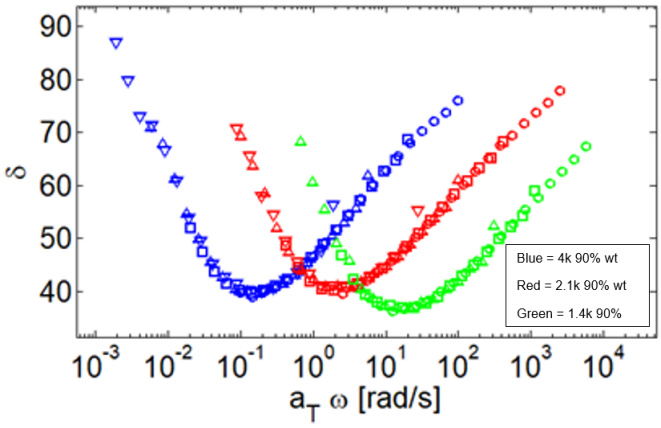

FIGURE 37 – Master curve of the phase angle δ for the bidisperse blends4k, 2.1k and 1.4k, at a reference temperature of 125°C.

The corresponding shift factors which have been used to build these master curves are shown in Figure 38 as a function of the experimental temperature. Their data are compared to the WLF equation found by considering that the samples have a Tg of 106.6°C and based on the C1 and C2 values used in [4] (see the black curve). As expected, the experimental shift factors do not superimpose to this WLF curve, which reflects their different glass transition temperatures, which must be taken into account in the analysis.

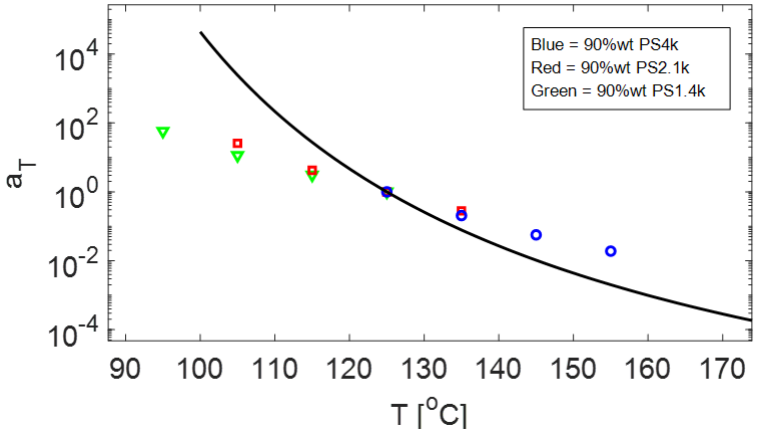

FIGURE 38 – Horizontal shift factors a_T determined by best fitting in order to build the master curves shown in Figure 3, for the three blends 4k, 2k and 1k, at a reference temperature of 125°C. The black curve represents the WLF equation for PS samples with a Tg of 106.6°C.

In order to account for the different Tg of the samples, the master curves must be plotted at different reference temperatures in order to be at iso-Tg condition, and ensure the samples have the same segmental dynamics. Since the Tg values found by DSC are 81.21, 65.92 and 47.79 for the blends 4k, 2k and 1k respectively, the reference temperatures should be chosen as equal to 104.6°C, 89.32°C, 91.58°C, and 71.19°C, which corresponds to a reference temperature of 130°C for a high

molar mass PS (with a Tg of 106.6°C), i.e. to $T - Tg = 23.4$°C. The corresponding shift factors are determined based on the WLF equation, in order to shift the data from 125°C to the new reference temperature. Results are shown in Figure 39, together with the blend 9k from ref. [4].

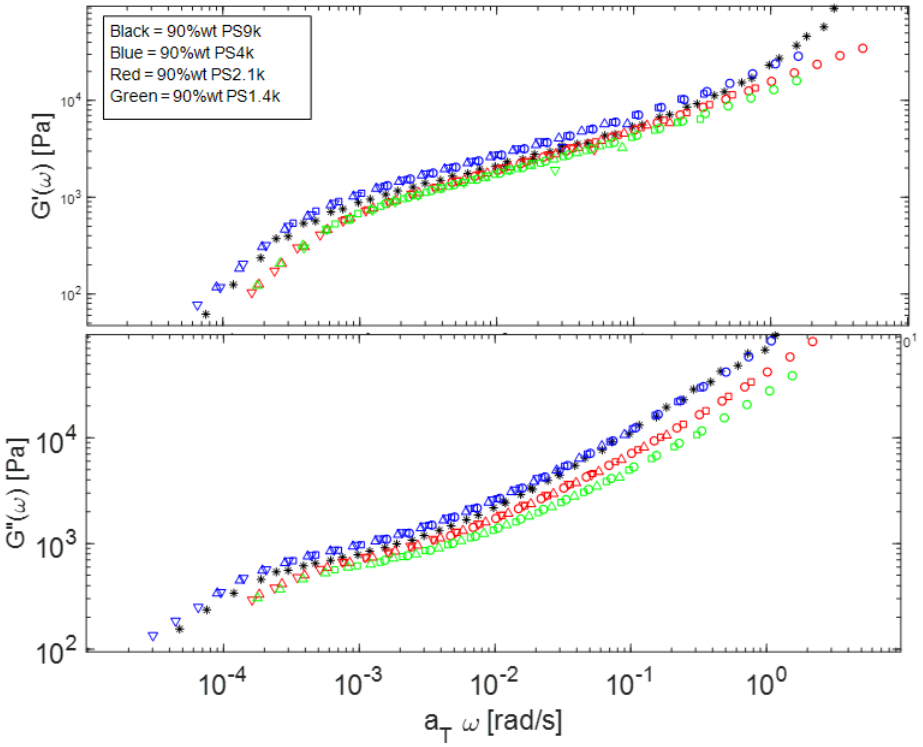

FIGURE 39 – Master curves of G' and G'' as a function of oscillation frequencies for the bidisperse blends 9k, 4k, 2.1k and 1.4k, under iso-Tg conditions. The reference temperature has been chosen such as $Tref - T_g = 23.4°C$.

It is observed that the data of blends 2k and 1k superimpose rather well, while a large discrepancy appears for the viscoelastic response of the blend 4k. In order to obtain a good superposition of the data, it is found that one should consider that this blend has a Tg higher than measured by DSC. In fact, one needs to ensure that the Tg value of the 4k blend is of around 19C higher than the glass transition temperature of the blends 2k and 1k. Taking the data of the blend 9k as reference, a good agreement is found if we consider that a Tg=84 °C, 64.92°C and 46.79°C for the blends 4k, 2k and 1k, respsectively. As shown in 40, a good agreement is found for all the curves, suggesting that the DSC data leads to a Tg which is 4°C too low for the blend 4k.

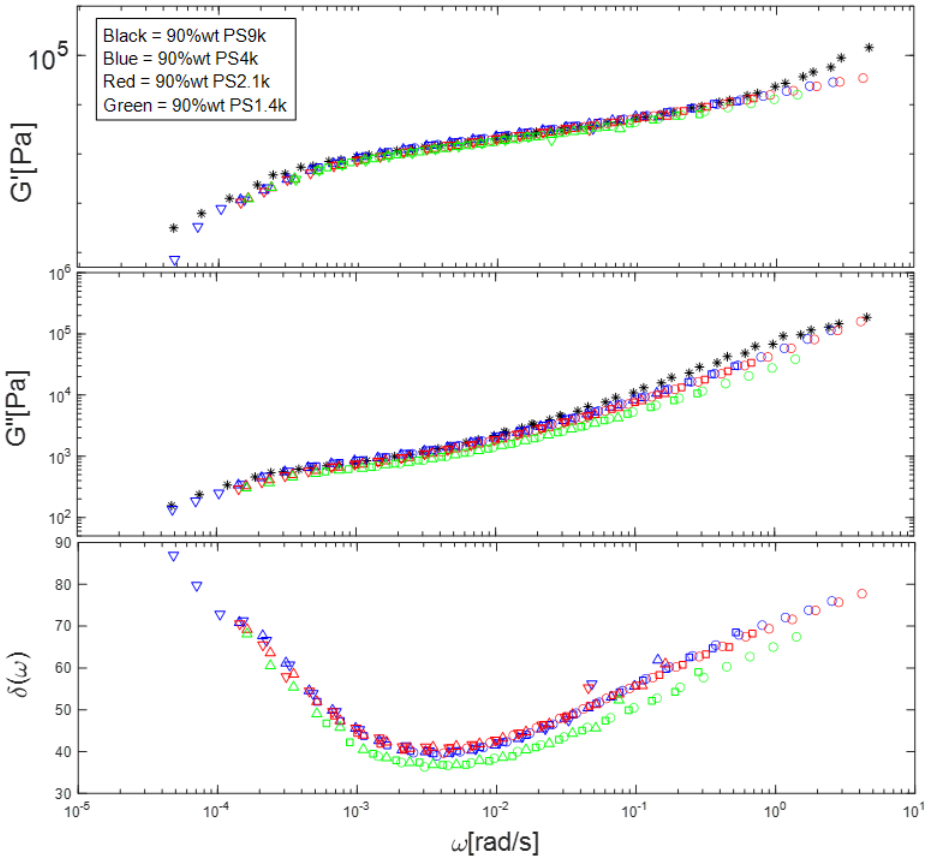

FIGURE 40 – Master curves of G' and G'' as a function of oscillation frequencies for the bidisperse blends 9k, 4k, 2.1k and 1.4k, under iso-Tg conditions. The reference temperature has been chosen such as $T_{ref} - T_g = 23.4$ °C. The T_g value of the blend 4k has been considered as equal to 84°C in place of 81.5C, while the Tg of the blends 2k and 1k have been considered as equal to 64.92 and 46.79 °C in place of 65.92 and 47.79 °C, respectively.

The corresponding shift factors used to build the master curves of Figure 40 are shown in Figure 41. In order to form is single WLF curve, these shift factors must be plotted as a function of $(T - Tg)$, as shown in Figure 42. The agreement between the curve is found to be good in general.

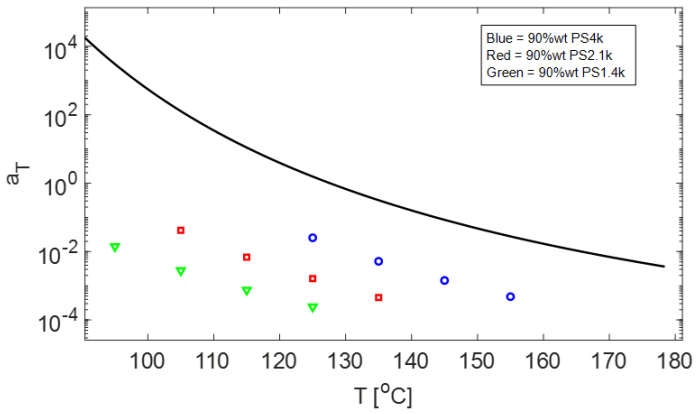

FIGURE 41 – Shift factors used to shift the experimental data to a reference temperature chosen to ensure that $Tref - T_g = 23.4°C$

.

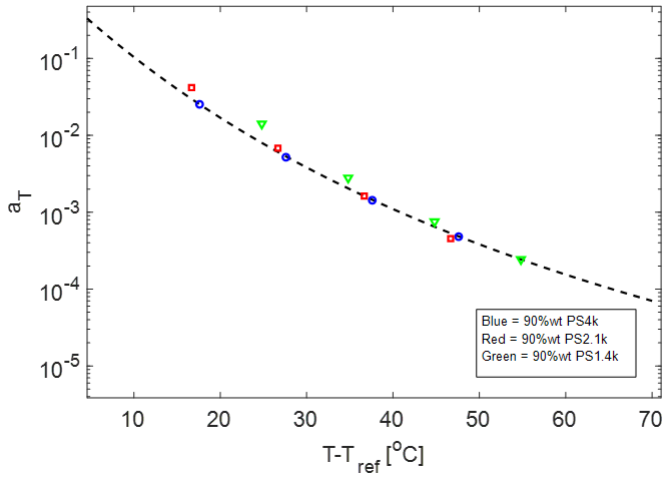

FIGURE 42 – Shift factors used to shift the experimental data to a reference temperature chosen to ensure that $Tref - T_g = 23.4°C$, plotted as a function of $(T - T_{ref})$

.

From this analysis, we can conclude that the Tg values obtained from the DSC curves do not allow to have consistent data in rheology, except if we consider that there is a discrepancy of 4°C either for the blend 4k or for the two other blends. This means that the difference in their Tg should be of 19°C, not of 15°C. This conclusion is further validated by looking at the raw viscoelastic data of the blends 4k and 2k, before any shifting: As shown in Figure 43, these two blends display very similar viscoelastic response when the measurement temperature differs by 20°C. This difference of 20 °C corresponds quite well to the predictions based on the Fox-Flory blending equation for the blends 4k and 2k. However, the Tg value by the latter equation is far too low and does not allow building a consistent master curve.

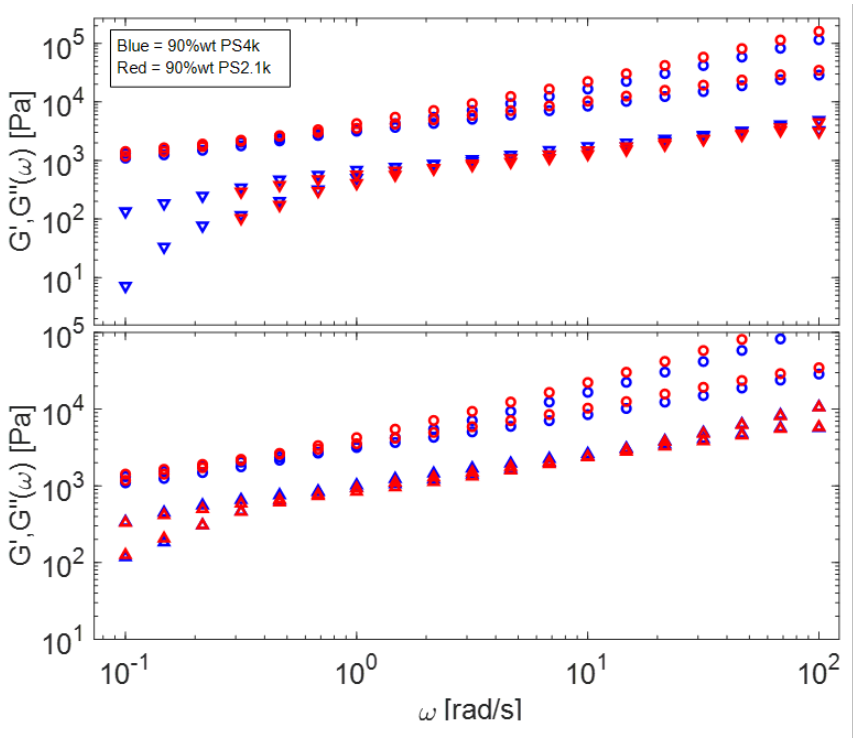

FIGURE 43 – Unshifted (raw) viscoelastic data of the blends 4k and 2k. Blue: 4k (o: 125C, □: 135C, △: 145C, ∇: 155C). Red: 2k (o: 105C, square: 115C, △: 125C, ∇: 135C).

Modelling the linear viscoelastic properties of the bidisperse blends

Master curves of G' and G" as a function of oscillation frequencies for the bidisperse blends 8.8k, 4k, 2.1k and 1.4k are compared with the curves predicted, based on the tube model, on Figure 44. Except for the plateau region where the modelling presents a lower value than what is experimentally obtained, there is a good correlation between the theoretical model based on the tube model (full curves) and the experimental results (symbols) for the lower and higher frequencies. The shift at the plateau region can however be justified by the model that considers the short chains are acting as a pure solvent. This assumption may be too strong as the oligomers need some time to relax and diffuse, possibly slowing down the motion of the long chains. This leads to a slight lowering of the plateau. Figure 44 (a) shows that a good agreement is obtained for the blend composed of very short matrix of mass 1.4kg/mol for the blend 1k.

Moreover, the more the oligomeric matrix is long, the more the deviation at intermediate frequency is large. We note, however, that for the blends 1k, 2k and 4k, the theoretical curves well predict the terminal regime, suggesting that for these blends, the oligomeric matrix can be considered as solvent when the time is long enough (t > 1000s). This is highlighted in Figure 44, which compares the viscoelastic responses of blend 1k and blend 4k compared with their predicted curve.

The material parameters used in the modelling have been fixed to: G_N^0=230000, Me=15000 and

τ_e=0.6

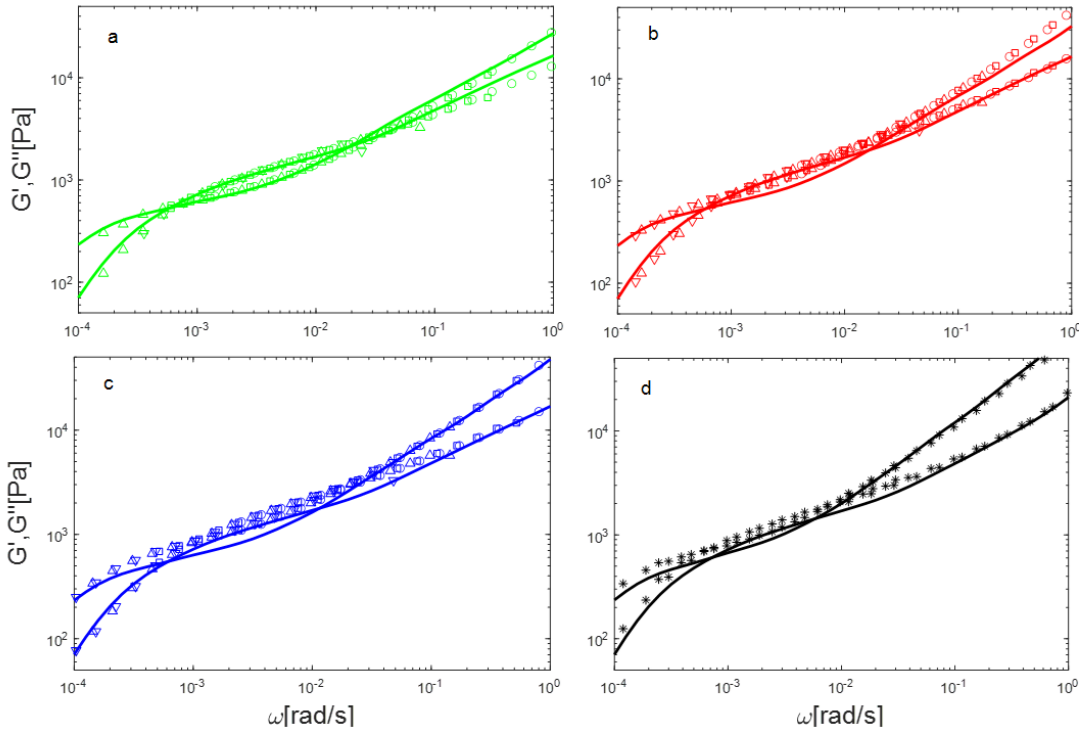

FIGURE 44 – Master curves of G' and G" as a function of oscillation frequencies for the bidisperse blends 90%wt 1.4k (green), 90%wt 2.1k (red), 90%wt 4k (green) and 90%wt 8.8k (black). Symbols are experiment data and full lines correspond to the modelization based on the tube model

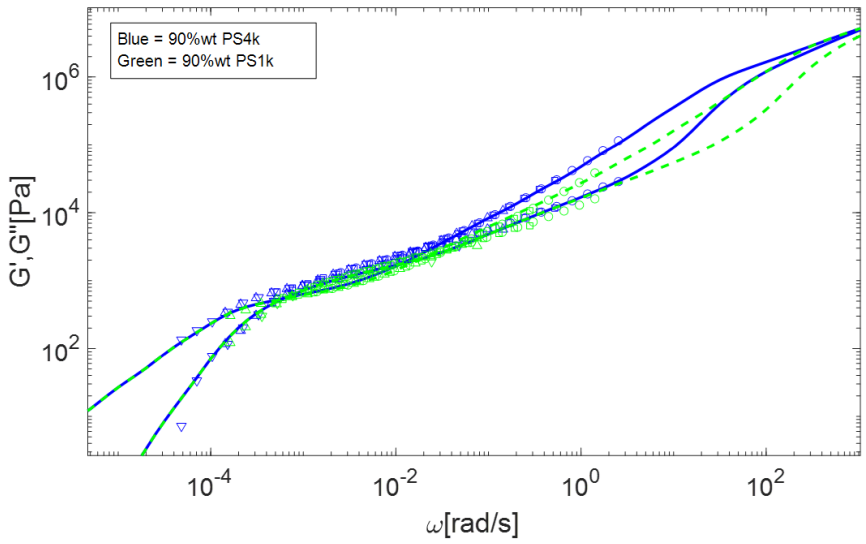

FIGURE 45 – Master curves of 90%wt PS1k (green) and 90%wt PS4k (blue) blends.

Figure 45 shows the predicted and experimental data of the blends 1k(green) and 4k (blue).

The high frequency region (frequency $>$ 0.1 rad/s) is mostly dominated by the relaxation of the oligomeric matrix. The latter relaxes through a Rouse process.
In the terminal regime, the data of both blends superimpose well. This regime is mostly dominated by the relaxation of the long chains of 820k polystyrene, which relaxes by reptation in a dilated tube formed by the entanglements between the long chains. Since both blends contain 10 wt% of long chains of same molar mass, their contribution to the viscoelastic data should be similar or even identical if the short matrix does not delay their relaxation.

In Figure 46, the predicted curves are decomposed into the contribution of the oligomeric matrix (see the dashed curves) and the contribution of the long chains (see the thin continuous curves), determined by assuming that the oligomeric matrix acts as a solvent. From this decomposition, we clearly see that the intermediate regime corresponds to the Rouse relaxation of the long entanglement segments (with the characteristic slopes for G' and G") followed, at lower frequency, by a plateau region. In its diluted state, the average molar mass between two entanglements along the long chain is estimated to be equal to (15 kg/mol)/0.1 = 150 kg/mol. This large value of the effective entanglement segments, which corresponds to a Rouse relaxation time of 0.55 s/$(0.1)^2$ = 55 s, explains why a Rouse process appears in this zone, well after the relaxation of the oligomeric matrix.

We also observe that for the blend 4k, this Rouse relaxation is slightly slower than predicted by assuming that the 4k oligomers behaves as a solvent. As already mentioned, this suggests that at short times, the oligomers slightly delay the long chain relaxation.

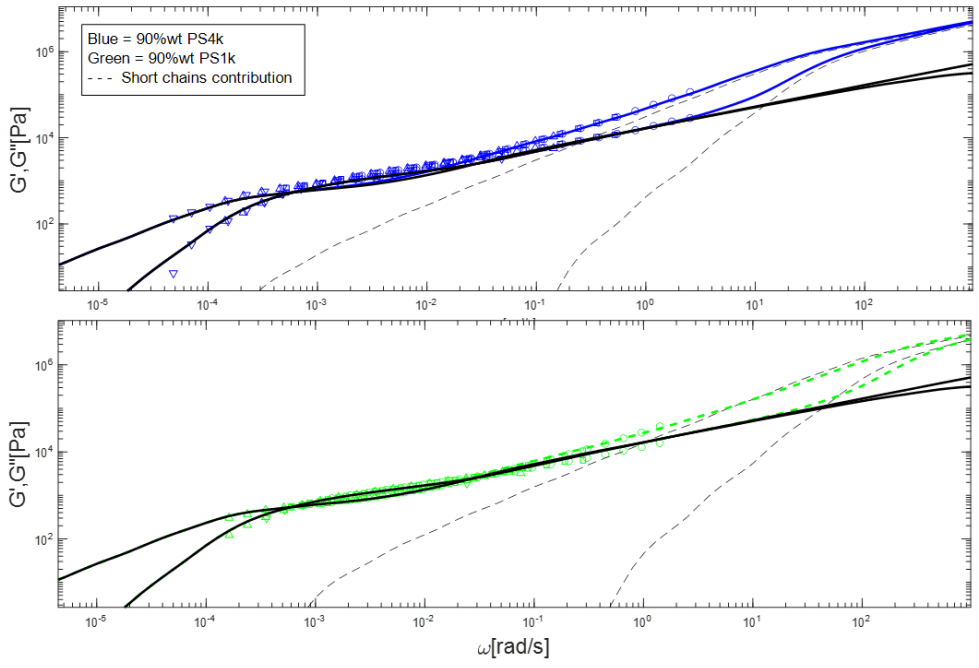

FIGURE 46 – Contribution of long (full lines) and short (dashed lines) component of master curves for 90%wt PS1k (green) and 90%wt PS4k (blue) blends.

As shown in Figure 44.d, the situation for the 90%wt PS9k blend is different: In this case, the delay observed at intermediate frequency is also observed at lower frequency in the terminal regime. This is attributed to the larger delaying effect of the oligomeric matrix 9k. In such a case, one cannot assume anymore that the short chains are similar to a solvent, even at long time. This delaying effect, similar to the one observed in ref. [[4]], can be accounted for by considering that the entanglement segments do not relax by an intrinsic Rouse process but rather by a slightly delayed Rouse, well represented by the Constraint Release Rouse process, i.e. a Rouse process taking place at the rhythm of the motions of the oligomers (see Section 2.3.2).

Figure 47 shows that, for the blend 9k, for which the size of the matrix is relatively high, we have to consider that the relaxation of long chains is delayed by a factor 1.4 through CRR (red curve), in comparison to its non delayed Rouse process (black curves).

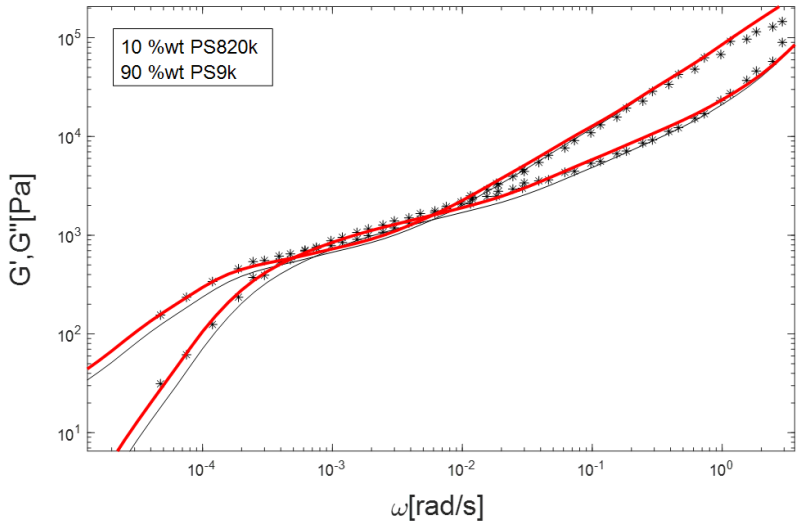

FIGURE 47 – Master curves of the 90%wt PS9k blend by considering (red curve) or not (black curve) the CRR relaxation mechanism.

The same reasoning applies for the tridisperse blends, composed of 10%wtPS820k / 33.5%wtPS4k / 56.5%wtPS34k. Its master curve is represented on Figure 48.

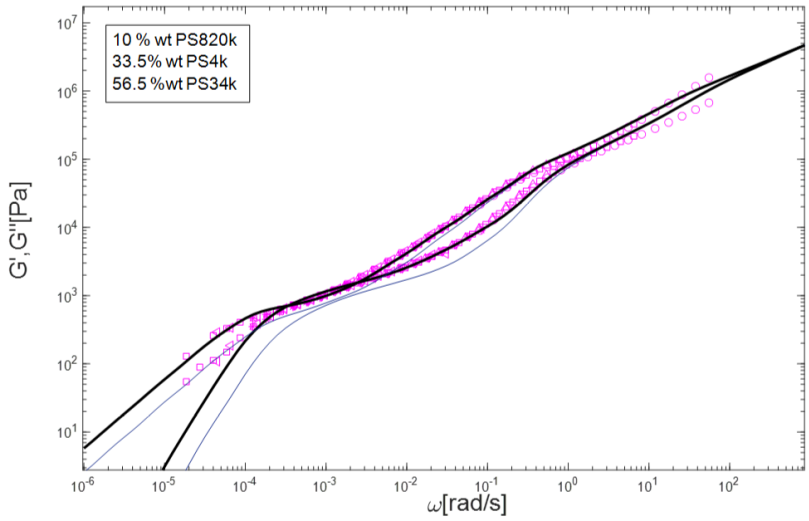

FIGURE 48 – Master curves of the 10%wt PS820k/33.5%wt PS4k/ 56.5%wt PS34k tridisperse blend by considering (black curve) or not (thin blue curve) the CRR relaxation mechanism.

It must be also noted that according to the DSC, the Tg of the tridisperse blend should be equal to 94.2 °C. This value is close to the value of 95.7 °C determined by using the Fox-Flory equation. As shown in Figure 48 and in the following figures, assuming $Tg = 94.2$ °C allows to build an accurate master curve. The data also showed a good agreement with the predicted data and with the experimental data of the bidisperse blends. So, based on the linear regime of deformation, the experimental value of Tg seems confirmed.

In Figure 48, the predictions obtained for the tridisperse blend by assuming that both the oligomer 4k and the chains 34k relax by a Rouse process, while the polymer PS820k relaxes first by Rouse up to its entanglements length scale, then by reptation, is also shown (See the thin blue curves). As expected, this leads to a too fast relaxation of the long chains. Similar to the 90%wt PS9k bidisperse blend, the longer matrix leads to a slowing down of the Rouse process of the long chains, which is better described by a Constraint Release Rouse process. For this situation a delay factor of 3 is found (i.e., the Rouse time of a segment between two long-long entanglements is equal to $3\tau_e/0.1^2$ rather than its intrinsic Rouse time, $\tau_e/0.1^2$. Accounting for this delay, a good agreement between the theoretical and experimental data is found. Nevertheless, a deviation is observed at low frequencies. This is attributed to an experimental issue, likely due to a too low signal from the instrument.

From these data, we conclude that once the difference in Tg is taken into account, the long chains relax 3 times slower in a matrix formed of 4k and 34k chains than in a real solvent or, equivalently, in a 1k oligomer. This delay is greater than in a 4k matrix (no delay on the terminal relaxation time) but is less important than in a matrix composed only of 34k chains.

Moreover, as shown in Figure 49, the long chains of the tridisperse mixture behave as in a bidisperse mixture with a chain matrix of molar mass of 23 kg/mol. The comparison is quite interesting because the average molar mass of the mixture (33.5% by weight of 4k + 56.5% by weight of 34k) is equal to 23 kg/mol. This result suggests that the delay effect on the relaxation of long chains is an average effect, depending on the average molar mass of the matrix. Although the fact that these two blends have a similar response, it should be noted however that the Tg of the two samples differs: the Tg of the 23K bidisperse mixture is 103.5 °C, while the T of the tridisperse mixture is 94.2 °C.

Finally, as already mentioned, we expect that the tridisperse blend has a Tg similar to the 90%wt PS9K (95.7 °C according to the Fox-Flory equation and 98.6 °C according to DSC) bidisperse mixture. It is therefore interesting to compare the viscoelastic response of the two blends, plotted at the same temperature.

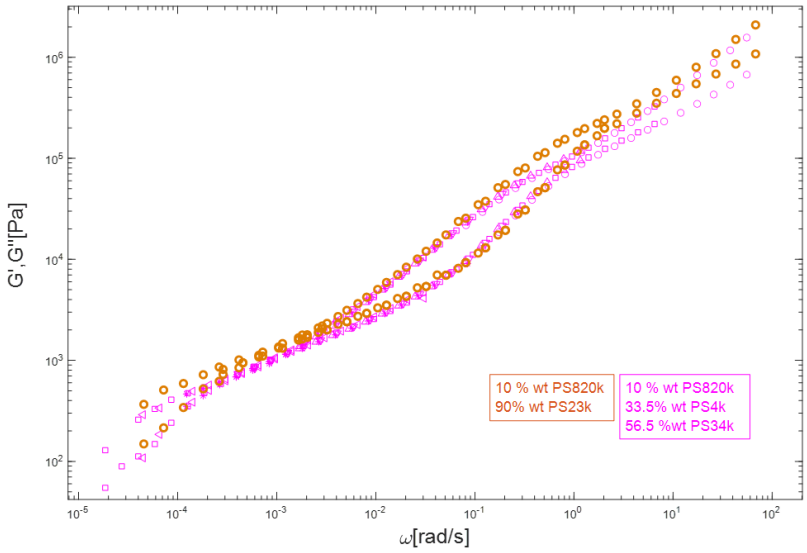

FIGURE 49 – Master curves for the 10%wt PS820k/33.5%wt PS4k/ 56.5%wt PS34k tridisperse blend (magenta) and for the 90%wt PS23k binary blend (orange, data from Taisir), and plotted at iso-Tg condition ($T - T_{ref} = 23.4$ °C).

Such comparison is shown in Figure 50. It is observed that the Rouse relaxation (stress) of the long chains is similar for both blends. Indeed, in the Rouse region of the long chains (from 1rad/s to 10rad/s), the data mostly overlap. However, at higher frequencies, the matrix containing the 34k chains relaxes more slowly. Additionally, at low frequency, the reptation of the long chains at 170°C is slightly slower for the tridisperse blend, due to the larger delay in CRR process.

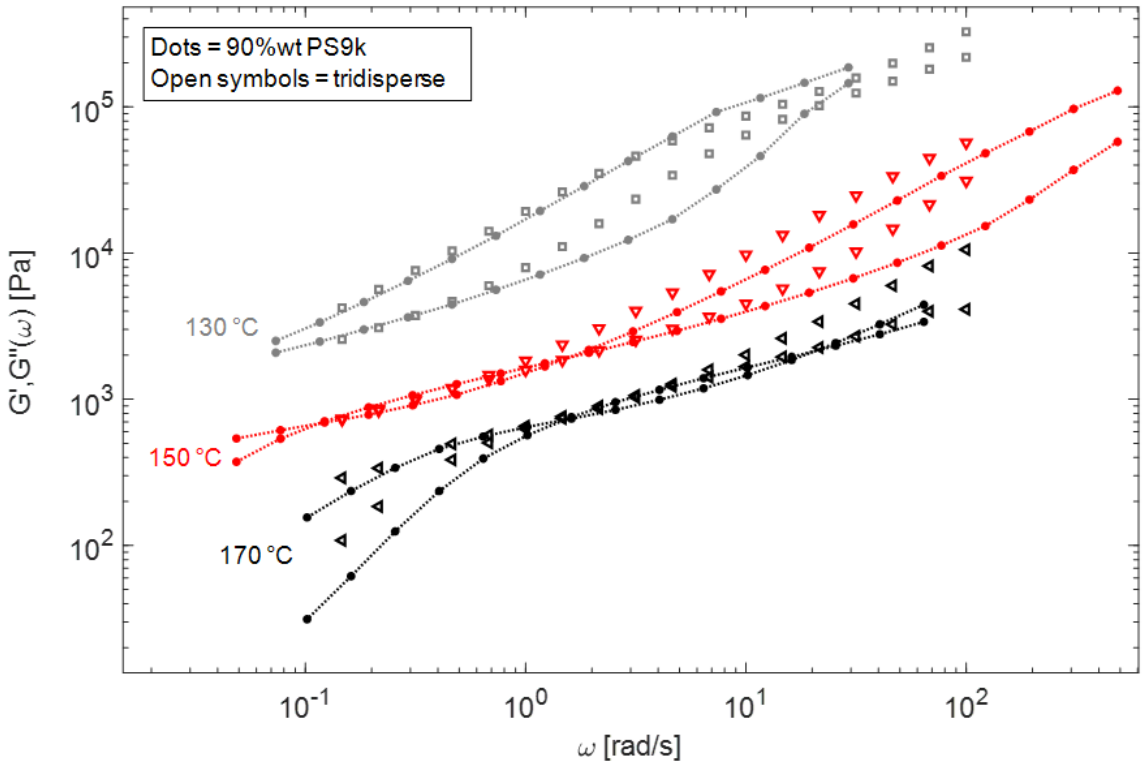

FIGURE 50 – Master curves of G' and G" for the 90%wt PS9k (dots) and for the tridisperse PS blend (open symbols) at 130°C, 150 °C and 170 °C.

In order to better highlight the CRR process and the delay of the relaxation of the long chains, compared to the bidisperse blend 1k, Figure 51 shows the master curves for the 90%wt PS9k (black) and the the 90%wt PS1k (green) binary blends, and for the 10%wt PS820k/33.5%wt PS4k/ 56.5%wt PS34k (magenta) tridisperse blend under iso-Tg conditions (T-Tg = 23.4C). The data should overlap at a very high frequency, before the Rouse relaxation of the 1K matrix,which is out of the experimental window. Then, the relaxation of the matrix is followed by the Rouse relaxation of the long-long entanglement segments and the reptation of long channels. In the upper panel, the delay in the long chain CRR process is clearly observed: the three mixtures display a similar relaxation, but have moved to a lower frequency if the long chains are diluted in a slower matrix. As observed in the lower panel of this Figure, the long chains relax 2 times slower in the tridisperse blend than in the 9K bidisperse blend.

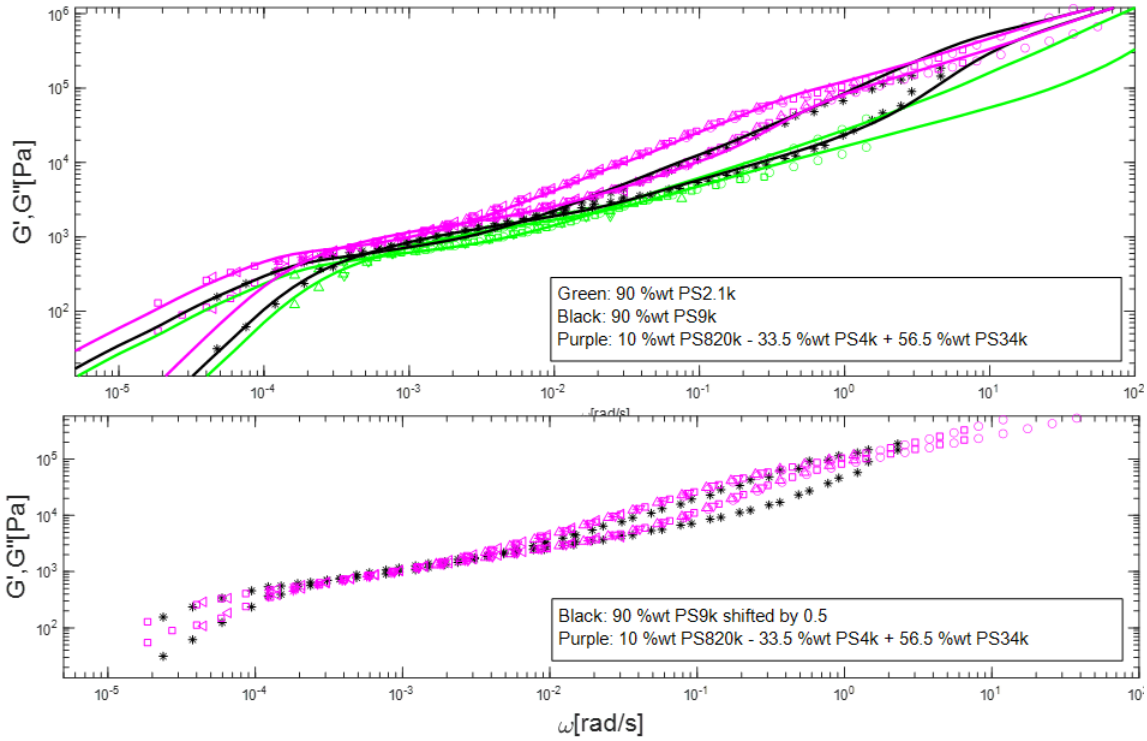

FIGURE 51 – Master curves for the 90%wt PS9k (black) and the the 90%wt PS1k (green) binary blends, and for the 10%wt PS820k/33.5%wt PS4k/ 56.5%wt PS34k (magenta) tridisperse blend.

The similarity observed in Figure 50 between the relaxation of the long channels diluted in a 9K matrix or in a matrix composed of 4K and 34K chains is attributed to two opposite effects: on one hand, the lower Tg of the tridisperse blend shift the data to a higher frequency, while, on the other hand, the stronger delay observed in the CRR process shift the data to a lower frequency.

To conclude this section, the linear viscoelastic responses of the different blends have been investigated and modelled, based on the tube approach. This allowed us to discuss the value of Tg. In particular, rheology data indicate that the Tg of the blend 4k is higher than measured. The data of the blend 9k have been modelled, based on $Tg = 98.6$C, as proposed by Shahid et al., but contrary to the theoretical value found with the Fox-Flory equation. Then, we have shown that for the blend 9k and the tridisperse blends, the Rouse relaxation process of the long chains is delayed, due to the slower motion of their longer matrix. This delay, estimated to 1.4 for the blend 9k and to 3 for the tridisperse blend, has been taken into account, based on the CRR mechanisms.

Based on this analysis, we can now investigate the properties of these blends under large deformation.

5.3 Viscoelastic response under uniaxial extension

Today, despite the great advantage of the filament stretching rheometer (VADER), the measurement of elongational properties of the melted polymer remains a difficult task. Many experimental problems can occur if the measurement parameters are not properly selected or if the sample is not properly placed in the rheometer. Figure 52 illustrates the main artefacts, which were observed during this project: first, at low rate, the force necessary to distort the sample becomes too low, which leads to inaccurate data. The feedback loop of the rheometer controls the stress to be applied to ensure that the diameter of the sample decreases with a constant Hencky strain rate. This leads to large oscillations in stress and a clear state of balance. Second, at high rate, it is possible that the thinning of the diameter of the sample becomes too important and deviates from a constant deformation speed. This leads to an underestimation of stress data. Such effect depends largely on the temperature: the latter must be low enough to reduce this additional thinning, but large enough to ensure a good adhesion of the sample to the plates of the rheometer.

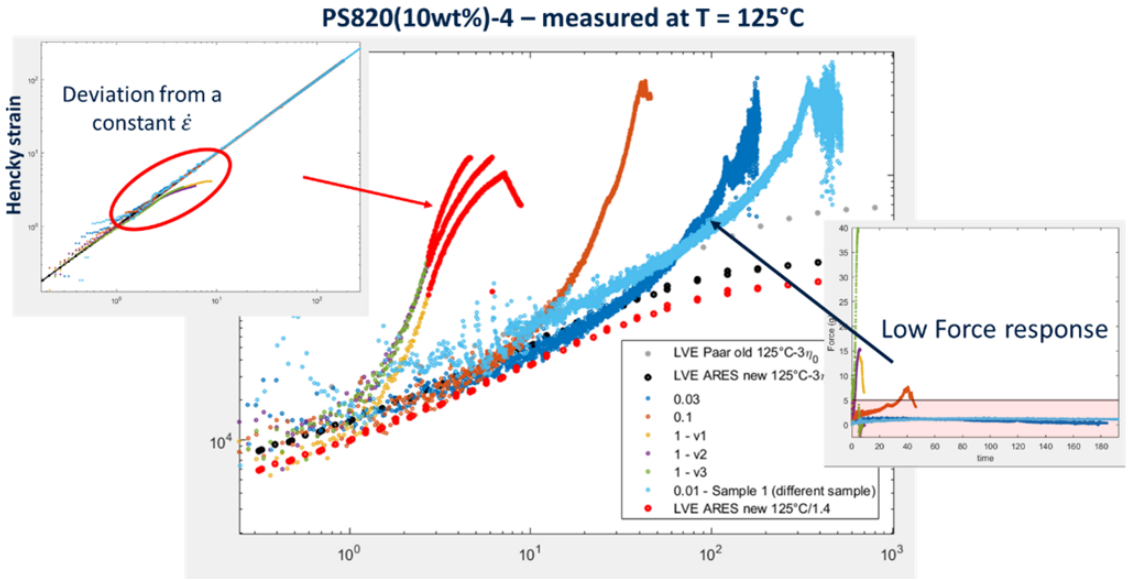

FIGURE 52 – Possible issues which could appears during the measurements

The influence of the temperature is illustrated in Figure 53. The 4K bidisperse mixture was measured at 115 °C (red curves) and 125 °C (green curves). In order to compare these data, the curves at 125 °C are shifted to a reference temperature of 115 °c, on the basis of the WLF equation (see equation 45). A WLF shift of 1/0.0148 is determined, which must be applied to the time from 125 °C to 115 °C, while a shift of 0.148 must be considered to rescale the strain rate.

The data obtained at a reference temperature of 115 °C is represented in the figure, as well as the linear envelope (see black dots), which comes from the storage and loss moduli. The curves seem to appear logically but only the data at Hencky deformation rates of 0.12/s and 0.148/s can be directly

compared because these deformation rates are very similar. It is observed that the data deformed at 0.148/s (measured at 125 °C) bends faster than the data at 0.12/s (measured at 115 °C). This comes from a too high measuring temperature.

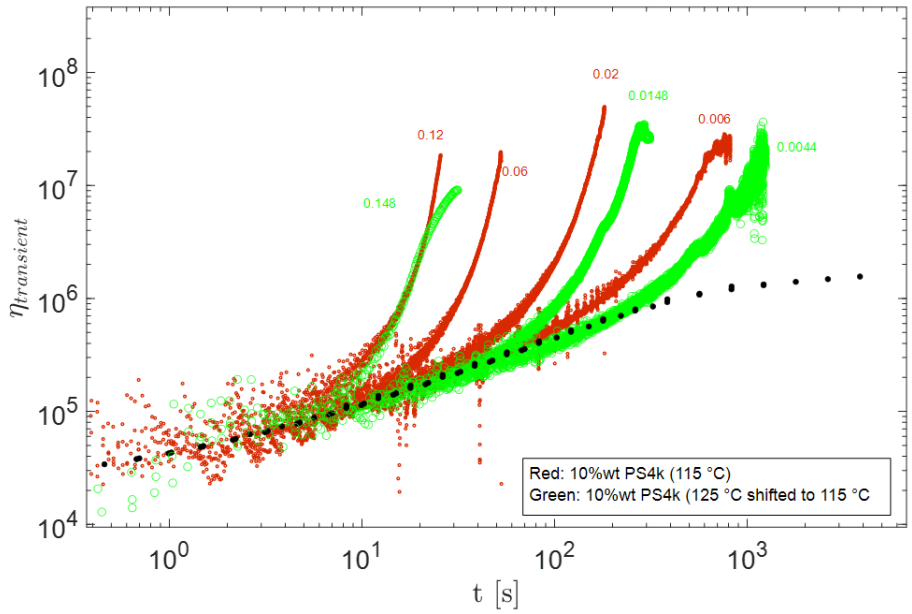

FIGURE 53 – Measurement of the 90%wt PS4K bidisperse mixture at 115 °C (red curves) and 125 °C (green curves)

Apart from at very low rate, the transient elongational curves did not reach their steady state value. This is due to the limit of the instrument, which fixed the maximum deformation that could be reached: At the end of the measurement, the samples, which are stretched in a filament, did not break.

The elongational data obtained for the 4k blend are compared to those of the 9k blend in Figure 54. From the linear viscoelastic data, it has been concluded that the glass transition temperature (Tg) of the 4k blend is 84°C, while the Tg of the 9k blend is 98.6°C. Iso-Tg conditions are thus achieved by plotting the 4k blend data at 115°C and the 9k blend data at $115°C + 98.6°C - 84°C = 129.6°C$. Since the original measurements were taken at 130°C, and the difference between 129.6°C and 130°C is minimal, and a temperature of 130°C has been selected for the comparison.

As shown on Figure 54, a good match between the data of the two blends is obtained, especially at a strain rate of 0.06/s for which the transient viscoelastic properties of both samples superimpose. This behaviour is expected since the strain hardening is only attributed to the stretch of the long chains. This good agreement validates the values used for their respective glass transition temperatures. However, while the 9k blend reaches its steady state, the 4k blend does not attain this level of deformation. Similar conclusions can be drawn for other strain rates. Again, the steady state was not reached with the 4k samples due to the limit of the instrument. It is probable that the

measurements of the blend 9k were performed with a lower amount of sample, in order to increase the range of deformation that can be reached by the rheometer.

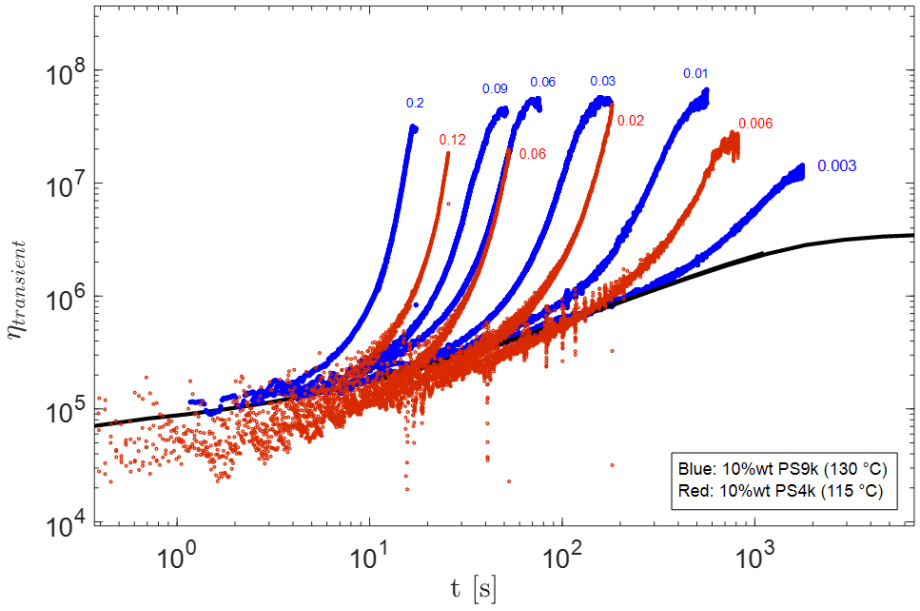

FIGURE 54 – Nonlinear data for 90%wt PS9k (blue) and 90%wt PS4k (red).

In Figure 55, the transient response of the 4k blend is compared to that of the 2k blend. To compare the curves, the latter, which has a Tg value of 65.92°C, should be plotted at a temperature of (115 °C - 84 °C + 64.92 °C = 95.92°C). Since the 2k blend was measured at 105°C, its data need to be shifted by a factor of 0.173 for the rate or 1/0.173 for the time.

Although the data of the two mixtures are similar, we observe that the strain hardening of the 2k mixture is slightly lower than that of the 4k mixture. This is well illustrated in this latest figure by comparing the rates of 0.06/s (for the 4k mix) and 0.052/s (for the 2k mix). This small gap is not visible in the corresponding linear envelope (see the dotted curves). Its origin is not clear and may be due to the slight delay observed at intermediate frequency (or, equivalently, intermediate strain rate) for the 4k mix due to a Constraint Release Rouse effect (see Figure 44).
Again, the transient data for the 2k mixture do not show a steady state for the same reason that for the 90%wt PS4k in Figure 54.

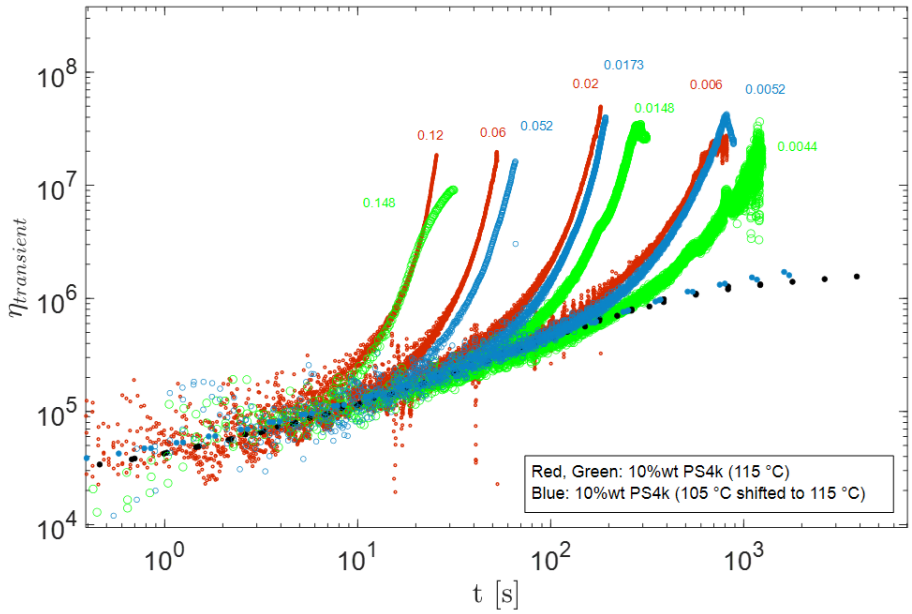

FIGURE 55 – 90%wt PS4k Blend (red and green) at 115 °C vs 90%wt PS2k (blue grey) at 95.9 °C to ensure iso-Tg condition.

Finally, we investigate the elongational data of the blend 1k. The latter has been measured at 95 °C, which is rather high compared to its Tg value (46.79 °C). As illustrated in Figure 56, this led to many experimental artefacts, which must be accounted for.

In order to compare these data with those of the other mixtures, the curves must be shifted to a temperature of 115 °C - 84 °C + 46.79 °C = 77.8 °C. This value is significantly lower than the experimental temperature of 95°C, which corresponds to a too liquid state of the sample. To correct this difference, a WLF offset of 0.047 (for strain rate) and 1/0.047 (for time) was applied. Reliable results are shown in Figure 57 (see orange data). There is also a curve that was measured at 105 °C and shifted to 77.8 °C based on an offset factor of 0.012 (see magenta data). Note that a good agreement is found with the other data.

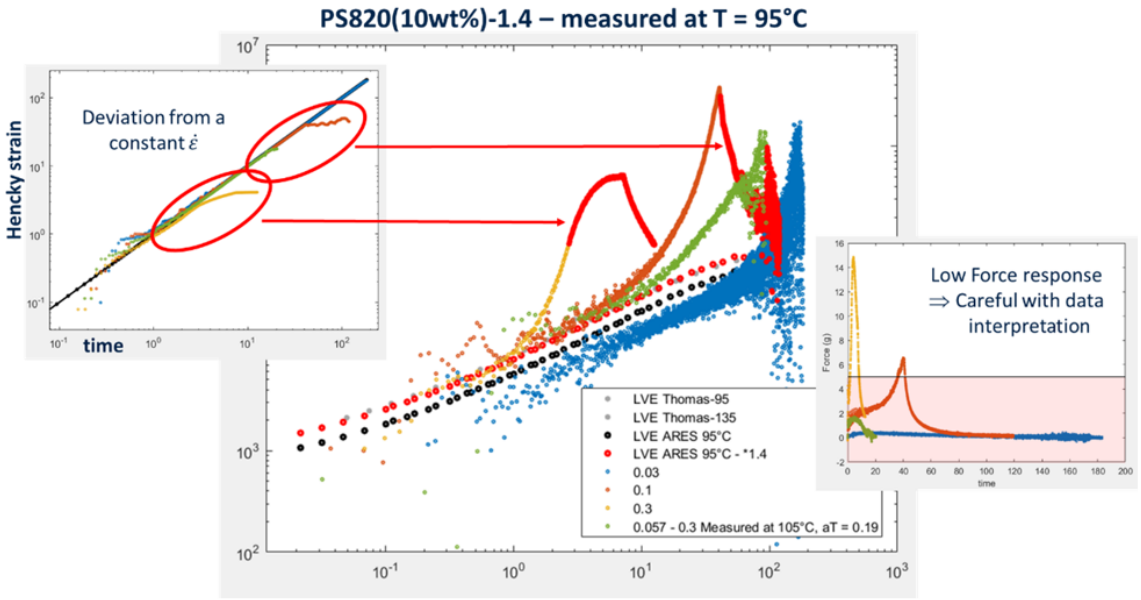

FIGURE 56 – Illustration of the experimental artefacts observed with the 90%wt PS1k blend.

Among these data, it is interesting to compare the different transient curves under the black arrow in Figure 57: We see that for a strain rate of approximately 0.005/s, the 1k mixture reaches a greater deformation than the 2k mixture, which reaches a larger deformation than the 4k mix.

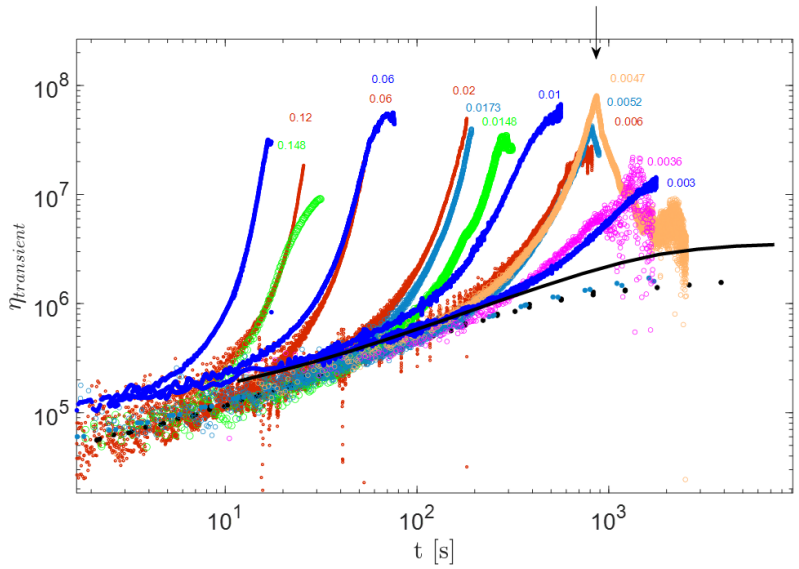

FIGURE 57 – Comparison of the nonlinear results obtained for the bidisperse blends, under iso-Tg conditions.

To conclude this part on the elongated properties of bidisperse mixtures, we note that significant

strain hardening is observed with all the mixtures. It is attributed to the stretching of the long chain (PS820k). The steady state is only observed for the 10%wt PS9k mixture. This is attributed to the use of another experimental protocol, based on a lower amount of sample, thus able to stretch up to larger deformation before reaching the limit of the device.

Based on these data, we cannot discuss the influence of the short chains matrix on the steady viscosity level because the latter is not reached.

Elongational properties of the tridisperse blend

We can now add the elongation data of our tridisperse blends. Its Tg value is equal to 94.2 °C and data have been measured at 130 °C. Therefore, to be compared to the bidisperse blends, these data must be shifted at a reference temperature of 115 °C - 84 °C + 94.2 °C = 125.2 °C, in order to ensure that ($T_{ref} - Tg$ = 31 °C). This corresponds to shifting the data by a factor 0.38 (for the rates) and 1/0.38 (for the time). Results are shown in Figure 58.

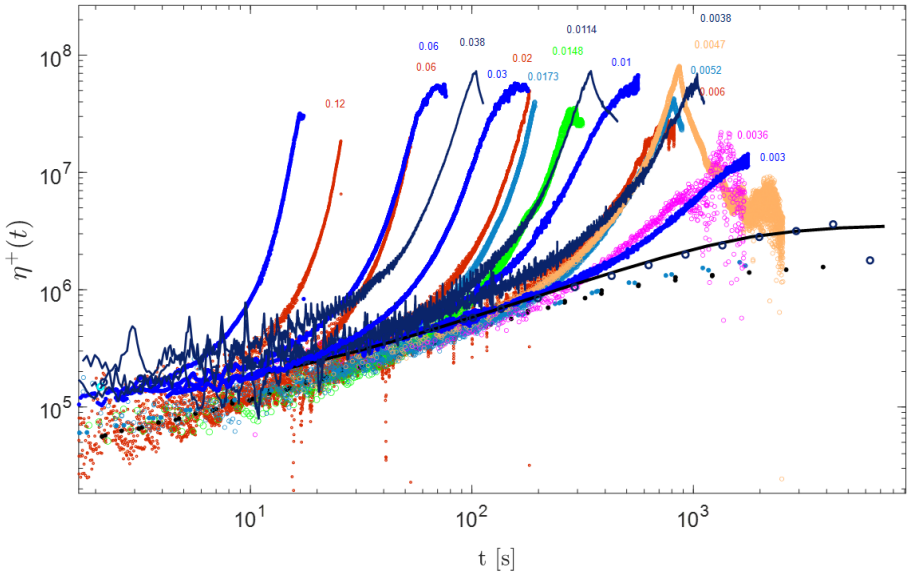

FIGURE 58 – Comparison of the nonlinear results obtained for the tridisperse sample (thin black curves) with those of the bidisperse blends (see above), under iso-Tg conditions.

In Figure 59, only the data of the tridisperse blend and of the blend 9k are shown, for a better comparison.

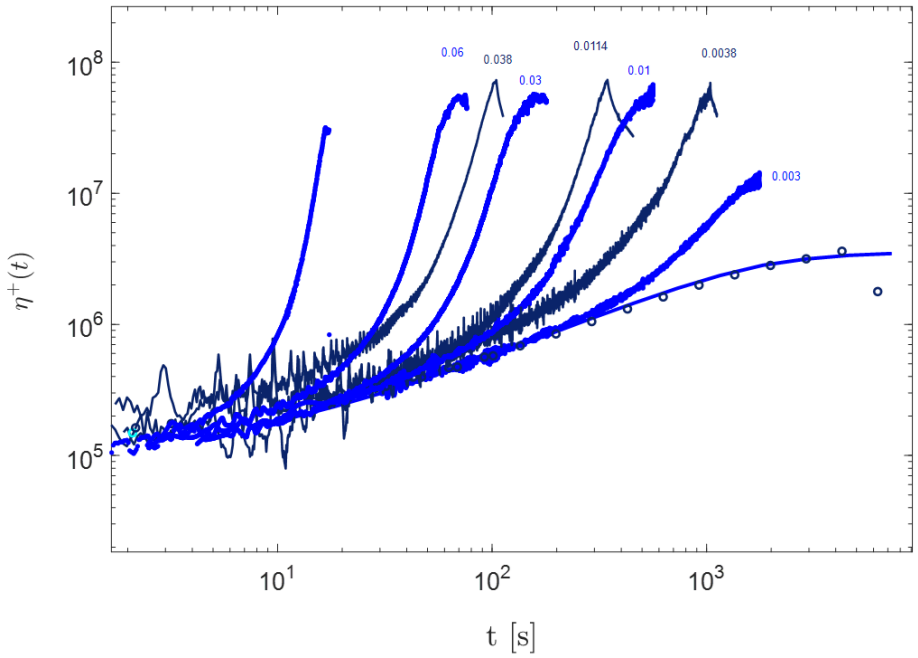

FIGURE 59 – Comparison of the nonlinear results for the tridisperse sample with those of the blend 9k at iso-Tg (i.e. at 130 °C for blend 9k and at 125.2 °C for the tridisperse blend).

Unlike bidisperse mixtures, the transient data from the tridisperse mixture do not appear to well match with the sequence of strain rates found by moving the data to iso-Tg conditions. Indeed, its strain hardening seems too strong for the rate applied. For example, when deformed at a strain rate of 0.0114/s, tridisperse blends behave almost like bidisperse blend deformed at 0.015/s. Unexpectedly, in order to obtain a good match between the data of the bidisperse blend 9k and those of the tridisperse blends, it is necessary to compare their elongational response at the same temperature T = 130 °C.
Indeed, as shown in Figure 61, when they are plotted in this way, their transient responses overlap. Such good overlap at 130 °C has already been observed in Figure 50, based on the storage and loss moduli of the mixtures. Today, this result cannot be explained, and raises many questions.

The most important one is the following: It is possible that the bidisperse blend 9k and the tridisperse blends have the same Tg ? This would explain, indeed, the results found in Figure 58.

Since the data of the blend 9k are consistent with the other bidisperse blends, it seems very improbable that its Tg value (98.6C) has been uncorrectly defined. Furthermore, in ref. [4], Shahid et al. found a good agreement with other bidisperse blends containing 10 wt% of PS820k, while using this value of Tg. Moreover, in ref. [18], Shahid et al. measured six different blends based on PS820k and PS9k, and their corresponding Tg values were found to all follow a linear dependence with the concentration of PS820k. So, to have the same Tg, this would mean that the Tg of the tridisperse blend should be of around 98.6 °C rather than of 94.2 °C. However, considering such a value of Tg does not allow to build a consistent master curve of the storage and loss moduli, as

shown in Figure 60. While using $Tg = 98.6$ °C allows obtaining a satisfactory superposition at low frequency, the data at high frequencies do not correctly overlap. Moreover, this value does not match with the DSC results.

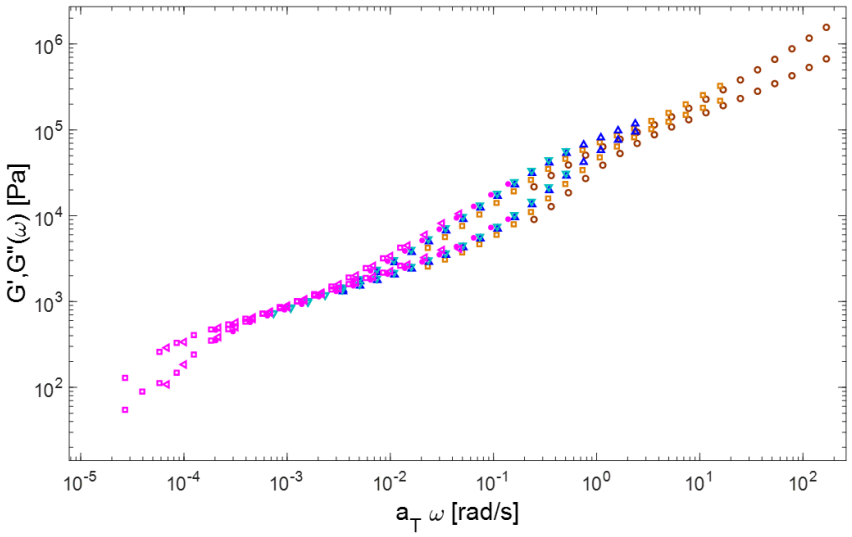

FIGURE 60 – Measurement of six different blends based on PS820k and PS9k by Shahid et al. [18]

Hence, from this comparison, it seems that both blends do not have the same Tg, as concluded in the previous sections. Starting from this assumption, this means that the elongation properties of the tridisperse blends cannot be explained based on its Tg value. The reason behind this conclusion is not clear. A possibility would be a stronger influence of PS34k, compared to the oligomer 1k, under large deformation, or an inhomogeneity of the blends at a very local length scale. This needs to be further investigated in the future, as it seems to demonstrate that the influence of Tg of the samples viscoelastic response may be different than expected, and possibly explains the breaking of the universal behaviour observed in literature for bidisperse blends in the nonlinear regime.

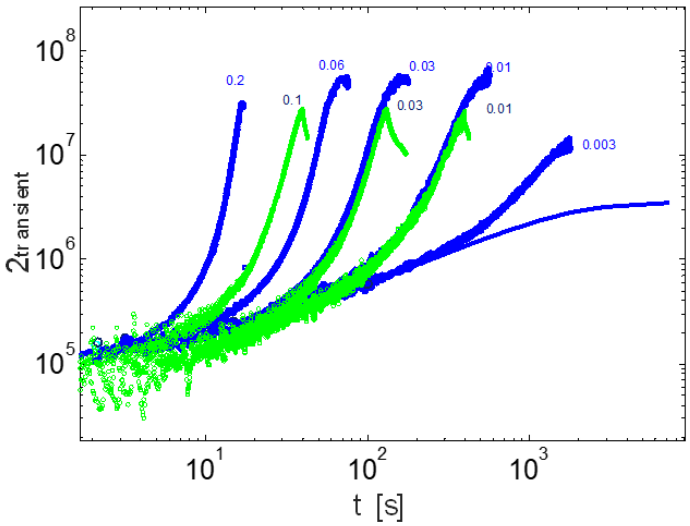

FIGURE 61 – Comparison of the nonlinear results for the tridisperse sample with those of the 90%wt PS9k blend at 130 °C

Hence, this result suggests that measuring at iso-Tg condition does not always ensure obtaining consistent data, as the Rouse process can be slightly delayed by the presence of the matrix.

6 Conclusion and perspectives

Obtaining rheological data in linear and extensional rheology for polymer samples is a complex task, requiring a meticulous and precise approach. These methods provide a valuable window into understanding the viscoelastic behaviour of polymers, but their sensitivity can make the interpretation of the results more challenging. As previously discussed, there is often little room for error between obtaining reliable results and raising further questions.

The results obtained in the context of this work, which is built upon findings from the literature, nevertheless raises some questions. These are discussed in this final concluding section.

■ The section on the study of the glass transition temperature leads to several conclusions:

The data plotted at a reference temperature of 125 °C show that the storage and loss moduli of the three bidisperse blends generally overlap but do not superimpose at high frequencies. This highlights the existence of different Tg values.

The phase angle δ, plotted against frequency, also demonstrates a good overlap of shifted data. When these shift factors are compared to the WLF equation, assuming a Tg of 106.6 °C, they do not align, emphasising once again the presence of different Tg values.

The application of the Fox-Flory equation, optimised using the Nelder-Mead minimization algorithm of Matlab, yields theoretical Tg values that align well with those determined by DSC for the 4k and 1.4k PS samples. However, for polymer blends, the theoretical Tg values based on the Fox-Flory relationship exhibit larger deviations from experimental data, particularly for blends containing the 2.1k and 1.4k PS samples.However, it is important to consider that, especially between 1000 and 10000 g/mol, the impact of minor imprecisions is significant.

■ The section on the linear viscoelastic properties of the bidisperse blends provided additional informations:

Adjusting the reference temperatures, the master curves of G" and G"" for the 2k and 1k blends superimpose well, but a significant discrepancy remains for the 4k blend. A good agreement is achieved when considering the Tg of the 4k blend as 84°C instead of 81.5°C. This adjustment aligns the viscoelastic response of all blends, suggesting that the DSC data for the 4k blend is 4°C too low. This finding is corroborated by the raw viscoelastic data, where the 4k and 2k blends show similar responses at a 20°C temperature difference (for a Tg of 84°C for the 4k blend and 64.9 °C for the 2k blend). This good agreement is confirmed by plotting the corresponding shift factors as a function of T-Tg.

The master curves of G' and G" for the 4k, 2k and 1k bidisperse blends with short oligomers show a strong correlation between the theoretical predictions and the experimental results. This observation holds true for most frequencies, with a deviation noted in the plateau region. The justification of this discrepancy is attributed to the assumption that short chains act purely as a solvent.

However, even though this interpretation seems to explain the linear viscoelastic behaviour of the 4k, 2k, and 1k blends, the scenario is notably different for the 90%wt PS9k blend: the delay observed at intermediate frequency extends to lower frequencies in the terminal regime and may be due to the larger delaying effect of the oligomeric matrix 9k. Consequently, one cannot assume that the short chains can be assimilated to a solvent, even at long time, but rather than entangled segments relax by constraint release Rouse (CRR), that taking place at the rhythm of the motions of the oligomers. The master curves derived from the experimental analysis seem to confirm this hypothesis.

Regarding the tridisperse blend, the Tg of 94.2 °C obtained from the DSC analysis coincides with the Tg of 95.7 °C obtained with the Fox-Flory equation. This good agreement is confirmed by the corresponding master curve. Furthermore, Similar to the 90%wt PS9k bidisperse blend, the longer matrix leads to a slowing down of the Rouse process of the long chains, which is better described by a Constraint Release Rouse process.

Moreover, the long chains of the tridisperse mixture behave as in a bidisperse mixture with a

chain matrix of molar mass of 23 kg/mol. This suggests that the delay effect on the relaxation of long chains is an average effect, depending on the average molar mass of the matrix. However, at higher frequencies, the matrix containing the 34k chains relaxes more slowly. Additionally, at low frequency, the reptation of the long chains at 170 °C is slightly slower for the tridisperse blend, due to the larger delay in CRR process.

■ The section on viscoelastic responses of bidisperse blends under uniaxial extension has taught us that the viscoelastic response under uniaxial extension shows significant strain hardening, attributed to the stretching of the long chain (PS820k). This has been observed with all the mixtures, even if the steady state is only observed for the 10%wt PS9k mixture. This latter scenario can be explained by the use of another experimental protocol, based on a lower amount of sample, that allowed to reach larger deformations before reaching the limit of the rheometer.

■ The section that examines the tridisperse mixture allows us to conclude the following: Concerning the tridisperse polystyrene blend, which includes short oligomers to maintain a high Tg, the experimental Tg closely matches the theoretical prediction, but the transient data from the tridisperse mixture presents a challenge as it does not align well with the sequence of strain rates typically observed under iso-Tg conditions.

Furthermore, despite being deformed at a rate of 0.0114/s, the tridisperse blends exhibit strain hardening comparable to bidisperse blends deformed at 0.015/s, indicating unexpected behaviour. This raises the question of whether the bidisperse 9k and the tridisperse blends share the same Tg. While it seems improbable that the Tg value of the bidisperse blend 9k (98.6° C) was incorrectly defined, previous studies have demonstrated a linear dependence of Tg on the concentration of PS820k. However, attempting to align the Tg of the tridisperse blend with that of the bidisperse blend 9k does not yield a consistent master curve of the storage and loss moduli, and does not align with DSC results.

Consequently, it appears that both blends do not share the same Tg, challenging previous assumptions. This suggests that the elongation properties of the tridisperse blends cannot be solely explained by their Tg value. Potential explanations include a stronger influence of PS34k compared to the oligomer 1k under large deformation, or blend inhomogeneity at a very local length scale. Further investigation is needed to understand why the influence of Tg on the viscoelastic response may differ from expected, and potentially explaining the deviation from universal behaviour observed in literature for bidisperse blends in the nonlinear regime. This outcome implies that obtain consistent data by measuring under iso-Tg conditions may not always be guaranteed, given that the presence of the matrix can slightly delay the Rouse process.

Références

[1] Brandon Khanyan Ronald P. D'Amelia*. An experimental review : Evaluation of the flory-fox equation for the relationship of glass transition temperature (tg) vs molar mass of polystyrene using differential scanning calorimetry (dsc). *Journal of Polymer and Biopolymer Physics Chemistry*, 10(81) :10–17, 2022.

[2] Saumya Madubhashini. Explaining the thermal behavior of polymers. *Polymer science adn technology*, 2022.

[3] Evelyne van Ruymbeke. *Polymer chains, LMAPR2018 Rheology.* Université Catholique de Louvain, 2024.

[4] Taisir Shahid, Christian Clasen, Filip Oosterlinck, and Evelyne van Ruymbeke. Diluting entangled polymers affects transient hardening but not their steady elongational viscosity. *Macromolecules*, 52(6) :2521–2530, 2019.

[5] Alexis André. Investigating the the linear and nonlinear rheology of model polymer melts (phd thesis). 2023.

[6] C-E Carels. *Dynamics of supramolecular entangled polymeric assemblies based on linear telechelic chains and metal-ligand interactions.* Université Catholique de Louvain, 2020. Master's Thesis.

[7] Maksim E. Shivokhin. *Understanding the effect of constraint release on the dynamics of entangled polymers.* Université Catholique de Louvain, 2014.

[8] C.-Y. Liu E. van Ruymbeke and C. Bailly. *Rheology Reviews , 53 - 134*, pages 53 – 134, 2007.

[9] ‡-¶ Salvatore Costanzo † ‡ Dimitris Vlassopoulos † ‡ Ralph H. Colby § Daniel Jon Read Hyojoon Lee Taihyun Chang Helen Lentzakis, † and Evelyne van Ruymbeke*. Constraint release mechanisms for h-polymers moving in linear matrices of varying molar masses. *Macromolecules, 52*, pages 3010–3028, 2019.

[10] C. ; van Ruymbeke E. Hannecart, C. ; Clasen. Constraint release rouse mechanisms in bidisperse linear polymers : nvestigation of the release time of a short-long entanglement. *Polymers 2023, 15, 1569.*, 2023.

[11] Qian Huang, Ludovica Hengeller, Nicolas J. Alvarez, and Ole Hassager. Bridging the gap between polymer melts and solutions in extensional rheology. *Macromolecules*, 48(12) :4158–4163, 2015.

[12] Giovanni Ianniruberto. Extensional flows of solutions of entangled polymers confirm reduction of friction coefficient. *Macromolecules*, 48(17) :6306–6312, 2015.

[13] ‡ ¶ Salvatore Costanzo † ‡ Dimitris Vlassopoulos † ‡ Ralph H. Colby § Daniel Jon Read Hyojoon Lee Taihyun Chang Helen Lentzakis, † and Evelyne van Ruymbeke*. Constraint release

mechanisms for h-polymers moving in linear matrices of varying molar masses. *Macromolecules, 52*, pages 3010–3028, 2019.

[14] Qian Huang, Olga Mednova, Henrik K. Rasmussen, Nicolas J. Alvarez, Anne L. Skov, Kristoffer Almdal, and Ole Hassager. Concentrated polymer solutions are different from melts : Role of entanglement molecular weight. *Macromolecules*, 46(12) :5026–5035, 2013.

[15] Qian Huang, Nicolas J. Alvarez, Yumi Matsumiya, Henrik K. Rasmussen, Hiroshi Watanabe, and Ole Hassager. Extensional rheology of entangled polystyrene solutions suggests importance of nematic interactions. *ACS Macro Letters*, 2(8) :741–744, 2013. PMID : 35606961.

[16] Hitachi. Dsc measurements of polystyrene. *TA Aplication brief*, Aug 1995.

[17] Roestamsjah. The glass transition temperature of monodispersed polystyrenes and their binary mixtures. *Journal of research of the National Bureau of Standards. Section A, Physics and chemistry*, pages 447–451, Jul-Aug 1974.

[18] T. Shahid, Q. Huang, F. Oosterlinck, C. Clasen, and E. van Ruymbeke. Dynamic dilution exponent in monodisperse entangled polymer solutions. *Soft Matter*, 13 :269–282, 2017.

UNIVERSITÉ CATHOLIQUE DE LOUVAIN
École polytechnique de Louvain
Rue Archimède, 1 bte L6.11.01, 1348 Louvain-la-Neuve, Belgique | **www.uclouvain.be/epl**